Neutron capture elements in the early Universe

Abdu Abohalima

Lund Observatory
Lund University

2017-EXA110

Degree project of 60 higher education credits (for a degree of Master)
May 2017

Supervisor: Louise Howes

Lund Observatory
Box 43
SE-221 00 Lund
Sweden

Acknowledgments

Completing this work would have not been possible without the help and support of my supervisor Louise Howes, to whom I am truly thankful. Her open door policy and thoughtful conversations helped me to develop tremendously. I am specially thankful for all the time and effort she put into proofreading and commenting on the different variants of this thesis, which with no doubt helped improve my scientific writing skills greatly.

I am also grateful to have received the Lund University Global scholarship that covered 100% of my tuition fees, making joining this program possible. I thank Dr. Gabriele Cescutti (I.N.A.F. Osservatorio Astronomico di Trieste) for providing us with the yields of his Galactic chemical evolution models and his beneficial comments on the results. I would also like to thank Brian Thorsbro for providing the wrapper for SME, and my neighbor Isak Svensson for his help with translating the Swedish summary.

Last but not least, I would like to thank everyone at Lund Observatory for providing a great scientific environment; my fellow master students and my office mates Kristiina Verro and Felix van Deelen for making this such a great experience.

Contents

Populärvetenskaplig sammanfattning

Varje stjärna vi ser på himlavalvet en stjärnklar natt tillhör vår galax Vintergatan, och var och en har de en historia att berätta. Målet med astronomi, den äldsta grenen av naturvetenskapen, är att förstå hur dessa magnifika strukturer uppstod och formades till den skepnad de antar i dag. Stjärnor bildas ur enorma gasmoln, och vid slutet av sin livstid slungar de ut sina beståndsdelar i galaxen. Denna process berikar galaxen med nya grundämnen. En stjärna fungerar som ett arkiv över de omständigheter som rådde i det medium ur vilket den skapades. Ur denna synvinkel kan de äldsta stjärnorna i vår galax betraktas som galaktiska fossiler, och genom att studera dem kan vi avslöja vår galax förflutna. Dessa uråldriga stjärnors atmosfärer har alla en gemensam kemisk egenskap: de uppvisar låga halter av metaller (det vill säga grundämnen tyngre än helium.) Ursprunget till denna egenskap är att de föddes vid en tid då endast ett fåtal tidigare stjärngenerationer hade fullbordats. Astronomer benämner dem som metallfattiga stjärnor, eller kortare ”MP” efter engelskans metal poor.

De bästa kandidaterna för att studera de äldsta epokerna är de första stjärnorna som någonsin uppstod, men dessa är tyvärr borta sedan länge. De näst bästa kandidaterna är de stjärnor som bildades av askan från den första generationen. Dessa stjärnor är de som vi i dag observerar som metallfattiga (MP) och gamla stjärnor, och de hjälper oss även att förstå de första stjärnornas natur. Likt arkeologer som avslöjar mänsklighetens historia genom att studera fossiler och artefakter skriver galaktiska arkeologer (astronomer som studerar de allra äldsta stjärnorna) vår galax tidigaste historia genom att leta efter de mest metallfattiga gamla stjärnorna.

I detta arbete mätte vi förekomsten av fyra tunga grundämnen (Sr, Y, Ba och Eu) i 48 MP-stjärnor som befinner sig i galaxens inre regioner (kallad utbuktningen.) Vi tror att dessa stjärnor är några av de äldsta som någonsin skådats. Genom att studera förekomsten av ovan nämnda grundämnen i de äldsta stjärnorna kan vi skapa en bättre bild över hur de bildades i universums barndom. Dessa tunga grundämnen bildas genom en process kallad neutroninfångning (n-capture), vilken kan delas in i två grenar kallad snabb process (r-process) och långsam process (s-process). Dessa grenar bidrar på var sitt sätt till produktionen av tunga ämnen. Syftet med detta arbete är att hjälpa till att identifiera var den tidiga produktionen av tunga element ägde rum. Denna information hjälper oss i sin tur att förstå hur de första stjärnorna var uppbyggda, samt hur de dog.

Det centrala resultatet av arbetet är att våra stjärnor mestadels beter sig likt MP-stjärnor från de yttre regionerna av galaxen, med vissa skillnader. Denna överensstämmelse mellan stjärnor från olika regioner betyder att den kemiska anrikningshistoriken är likartad. Vi jämförde även våra resultat med vissa teoretiska modeller som förutspår en möjlig produktionsplats för dessa ämnen. Resultaten från jämförelsen visar att mer arbete behövs för att förbättra modellernas överensstämmelse med empiriska observationer. Det saknas ännu förståelse för hur lätta grundämnen producerades genom neutroninfångning i det tidiga universumet.

Abstract

Metal-poor (MP) stars in the Milky Way (the Galaxy) and its satellite galaxies open a window into the earliest times in the history of the Universe, probing the chemistry of the earliest times. Recent galaxy formation simulations predict that the oldest MP stars are those on tightly bound orbits in the inner regions of a galaxy (Tumlinson 2010). Applying this to the Milky Way, MP stars in the bulge would have a higher probability to have formed at higher redshifts compared to MP halo stars.

In this work we have measured the abundances of Sr, Y, Ba and Eu in 48 MP stars from the inner regions of the Galaxy. This is the first time neutron-capture elements have been studied for a significant sample of stars in the bulge. Our results show that the bulge sample generally behaves similarly to the halo stars, with some differences. We find an increasing scatter in the abundances of Sr and Ba with decreasing metallicity as in halo stars, this is not the case for Y and Eu where our stars show a constant scatter scale. As reported in François et al. (2007) for their sample, we find an anticorrelation between [Y/Sr] and [Sr/H], this is not seen in other halo samples, more stars at the lowest metallicities are needed to confirm this behavior. Our stars are on average r-enhanced compared to the halo stars with $\sim$50% of the stars having [Eu/Fe]$>$ 0.6, favoring r-process production sites with high yields such as neutron star mergers and magnetorotationally driven supernovae. We find one star with exceptionally high [Sr/Ba]=2.04 and [Y/Ba]= 1.72 that is slightly carbon enhanced with [C/Fe]=0.65. This star could be in a binary system, only a handful of stars from the literature show similar values.

Similar to halo MP stars, we find an anticorrelation between the abundances of the light s-process (ls) elements Sr and Y and the heavy s-process (hs) element Ba. This behavior is not explained using the yields from the main r-process only. We compare our results to Galactic chemical evolution models (one for the halo and another for an old bulge population) that include massive fast-rotating stars (spinstars) as a production site for ls elements at the earliest times along with the main r-process from magnetorotationally driven supernovae. The results from this comparison show that the halo model better matches our data than the bulge model. However, more work on the spinstar models is needed to better predict the trends from our stars. The source of ls elements in the early Universe remains unknown for the time being.

Chapter 1

Introduction

Studying the oldest stars in the Milky Way is of great importance to astronomers, both theorists and observers. There are mainly two sources that enable us to observe the early Universe, either galaxies at very high redshifts or very old stars that date back to the earliest times in the Universe. To study the detailed chemistry and physics of the earliest times, these nearby stars are the best candidates. A star's atmosphere preserves the conditions of the medium from which it was born, keeping a record of the previous generation's element production. Old stars give us direct access to the chemical and physical conditions of the interstellar medium at their birth time, given we can find them. These old stars have one common property, that they all lack metals (elements heavier than He) in their atmosphere, astronomers label them as metal-poor (MP) stars.

We first start by discussing the importance and use of MP stars in astronomy, then we explain what neutron capture elements are and their possible production sites in the early Universe, this then leads us to the question where the oldest stars are today in the Milky Way and how astronomers can hunt them down. We end this chapter with the aims of this project and the outline of this thesis.

1.1 Metal-Poor Stars

MP stars are our window to the early times in the Universe. As ages of stars in general can not be determined precisely yet, a general assumption is that the more MP a star is, the older it is expected to be. Hence in general astronomers use the lack of metals as an indicator that a star is old. Chemical abundances in the atmospheres of stars act as a record preserving the chemical properties of the star's birth environment. In MP stars this record can date back to the very first stars that formed after the Big Bang. The interest in MP stars has been extremely high over the past three decades, with the number of discovered stars increasing rapidly with time (Christlieb et al. 2002; Frebel et al. 2005; Caffau et al. 2011; Keller et al. 2014). The aim of such studies is to understand the formation of the first stars and how MP stars can be used to constrain their properties (Frebel and Norris 2015).

Studying the abundances of elements in the oldest stars gives some insights into the properties of the first stars, usually referred to as population III (Pop III) stars. Pop III stars were responsible for the first metal enrichment of the interstellar medium (ISM). Pop III stars first started forming about 200 Myr after the Big Bang (Bromm and Larson 2004). At that time the Universe was free of elements heavier than lithium (formed through Big Bang nucleosynthesis), making them metal-free stars. Until recently Pop III stars were assumed to be massive short lived stars. However, recent studies show that Pop III stars might have formed at lower masses ($\leqslant 1 M_{\odot}$), and so could survive until now (Stacy and Bromm 2014). These old survivors would give us direct access to the chemical properties of the early Universe if we could find them. None have been found so far. To find the oldest survivors we need to study the stars that currently reside in the oldest components of the Milky Way (Tumlinson 2010).

The MP stars we observe today mostly formed a few generations after Pop III stars, though being MP does not directly mean the star is old, as we discuss in Section 1.4. Hence the properties found for MP stars do not necessarily relate to the earliest times in the Galaxy's history. To truly map the chemical evolution of the early Universe we need to find true old survivors from the earliest times. Nevertheless, theorists have used the chemical properties of MP stars to simulate the chemical evolution of the Galaxy. Thus finding and studying the properties of truly old MP stars would enhance these theoretical models, getting us closer to understanding the nature of the first stars and the early Universe.

1.2 Neutron capture elements

Elemental formation processes in the Universe can be divided broadly into 3 main categories; 1-Big Bang nucleosynthesis, responsible for the formation of hydrogen, helium and traces of lithium, this process took place in the first few seconds after the Big Bang. 2-Stellar nucleosynthesis in centers of stars, this process forms elements with atomic numbers $2 < Z \leqslant 30$ through nuclear fusion. 3-The neutron-capture process (n-capture), this process takes place in environments with high neutron fluxes (stars during the asymptotic giant branch (AGB) phase, neutron star mergers or core-collapse supernovae), forming elements with atomic numbers $Z > 30$.

The n-capture process is responsible for forming about 60% of the elements in the periodic table. Hence detailed studies of this process is of great interest to astronomers. The n-capture process is divided into two main mechanisms depending on the rate at which neutrons are captured by the nucleus of an Fe-peak atom (elements with atomic numbers $21 \leqslant Z \leqslant 30$), the slow n-capture process (s-process) and the rapid n-capture process (r-process). Each of these processes has a different production site that is more efficient in producing certain elements. The main s-process takes place in stars during the AGB phase of stellar evolution (for a review of the subject see Busso et al. 1999). The production sites of the r-process are not confirmed so far, two possible sites are neutron star (NS) mergers (Freiburghaus et al. 1999) and during core collapse supernovae (CCSNe)

(Cowan and Thielemann 2004, and references therein).

These two processes produce heavy elements with different ratios. No element is formed solely due to one process, depending on which process is dominant the element is then categorized as an *r*-process or *s*-process element. By measuring the relative abundances of the elements in a star, it is possible to infer which process was responsible for forming the heavy elements measured. The contribution from the main s-process to the Solar system material has been estimated using stellar models (Arlandini et al. 1999; Travaglio et al. 2004). By subtracting the s-process fraction from the total of the Solar abundances, the r-process contribution can be estimated as well (Arlandini et al. 1999; Sneden et al. 2008). These studies present the contribution ratio of each process to the production of heavy elements.

Massive, short lived stars die as CCSNe after only a few Myrs. In contrast, the AGB phase of stellar evolution takes place in low to intermediate mass stars ($0.7M_{\odot} \leqslant M_{*} \leqslant 10M_{\odot}$). It takes longer (on the scale of *Gyrs*) for these low mass stars to evolve off the main sequence up to the AGB phase. As they are the main source of *s*-process elements, the ISM is not enriched in *s*-process elements for at least 1 *Gyr* (Busso et al. 1999). Hence the *r*-process is the main source of elements heavier than Fe in the early Universe. Another n-capture process in massive stars is the weak *s*-process that takes place at the end of helium and carbon burning in the core of these massive stars. This process produces elements heavier than Fe up to strontium (Sr) & yttrium (Y), therefore contributing to the abundances of *s*-process elements. This process is secondary, with its production efficiency decreasing with metallicity (Käppeler et al. 2011, and references therein).

From this, we would expect old MP stars to be deficient in *s*-process elements, only with low abundances that may arise from the weak *s*-process in massive stars, and from the *r*-process. In the last few years the abundances of n-capture elements have been measured for a large sample of MP stars from the halo of the Galaxy (Yong et al. 2013; Roederer et al. 2014; Barklem et al. 2005). These abundance studies show that some of these stars are enhanced in *s*-process elements (Chiappini et al. 2011; Barbuy et al. 2009), while other stars show a spread and anticorrelation in the abundance ratios of light to heavy *s*-process elements (François et al. 2007). These stars are expected to be old and should have formed at a time when the Galaxy was poor in *s*-process elements. Chemical evolution models of the Galaxy that include feedback from the *r*-process only, on short timescales fail to explain these values (Cescutti et al. 2013).

The scatter between light *s*-process elements and heavy ones, for example the [Sr/Ba][1] spread needs another process that enhances the early Universe with light *s*-process elements. Many suggestions exist in the literature for this unidentified process. One that we test in this work are massive fast-rotating stars (often called spinstars), as a secondary production site for *s*-process elements over short timescales (discussed in Section 1.3). In order to test the possible origins of this early *s*-process production we need to find and study the chemistry of the oldest stars in the Galaxy, but first, what are spinstars? and

[1]The expression [X/Y] denotes the relative abundance of element X to element Y in the star compared to that of the Sun, where [X/Y]=0 for the Sun. $[X/Y] = \log_{10}\left(\frac{N_X}{N_Y}\right)_{*} - \log_{10}\left(\frac{N_X}{N_Y}\right)_{\odot}$.

how do they contribute to the s-process abundances?

1.3 Early s-process production (Spinstars)

Spinstars are massive stars that have high rotational velocities ($500 - 800$ km/s), these high velocities are predicted due to them being metal-free/poor. Spin-stars are theoretically modeled stars, we do not see any today to confirm their existence. Recent theoretical models (Cescutti et al. 2013; Cescutti and Chiappini 2014) show that spinstars are able to boost the s-process yields by up to 4 orders of magnitude (Pignatari et al. 2008; Chiappini et al. 2011). Since massive stars are short-lived, this will enrich the ISM with light s-process elements over short timescales. The models of spinstars also show an enhancement in the production of the CNO elements, carbon, nitrogen and oxygen.

Massive stars during the He burning phase consist of a core burning He to C, the core is surrounded by a H burning layer. The ^{12}C that is formed in the He burning core is brought into contact with the bottom of the H-rich layer due to internal mixing induced by the fast rotation. This process converts ^{12}C into ^{14}N through the CNO cycle. This produces a large amount of ^{14}N.

The ^{14}N formed at the edge of the He burning core is mixed back into the core and transformed to ^{22}Ne through the α-capture sequence. ^{22}Ne through the reaction $^{22}\mathrm{Ne}(\alpha, n)^{25}\mathrm{Mg}$ acts as a neutron source for the n-capture process to take place (Maeder and Meynet 2012). The neutrons released through the $^{22}\mathrm{Ne}(\alpha, n)^{25}\mathrm{Mg}$ reaction are captured by the nuclei of Fe-peak elements. This process can form light s-process elements. The production of s-process elements depends on the amount of ^{22}Ne and Fe-peak elements. The s-process in spinstars could make these stars a source of light s-process elements in the early Universe.

The existence of these spinstars in the early Universe has several expected signatures, one of which is an early enrichment in light s-process elements Sr and Y. This enrichment is seen as a scatter in the abundance ratios of elements from the different s-process peaks (Sr, Ba & Pb). These elements with a magic number of neutrons are very stable against neutron capture, and so large abundances are built up. Models that include the feedback from spinstars with the standard r-process enrichment are in good agreement with observations in the halo of the Galaxy (Cescutti et al. 2013). However, as halo MP stars formed over a large range of times, we can not confirm that the enhancement is not from AGB enrichment instead. Hence we need a MP sample that is truly old in order to check for the existence of spinstars amongst the first stars. This takes us to our next point, where are the oldest stars today? and can we find them?

1.4 Where are the oldest stars?

To answer this question we need to understand how the Galaxy formed and evolved to what we observe today. Recent cosmological simulations model the process of galaxy formation through a hierarchical growth pattern (White and Springel 2000; Diemand et al.

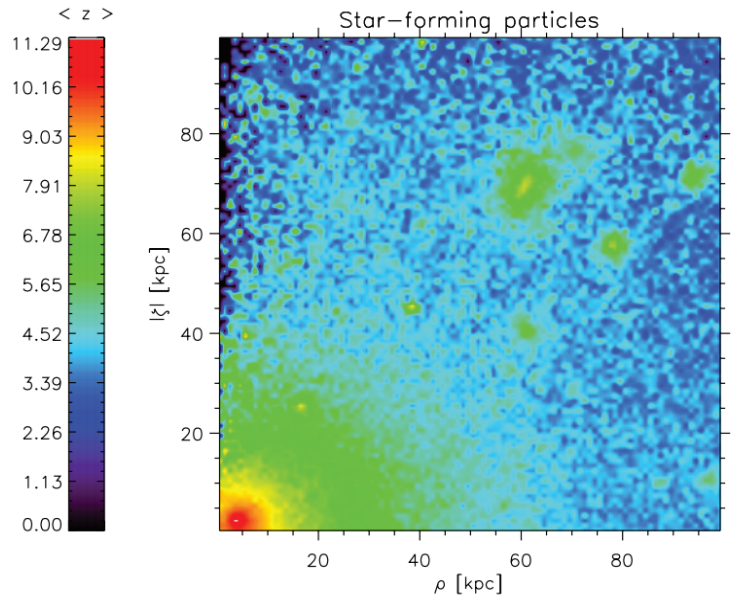

Figure 1.1: Figure 4 from Salvadori et al. (2010). The formation redshift of dark matter particles hosting stars with $[Fe/H] < -1$. The formation redshift increases with decreasing distance from the Galactic Center.

2005; Salvadori et al. 2010; Tumlinson 2010; Starkenburg et al. 2017). These simulations include baryonic matter with dark matter to map the distribution of old stellar populations and focus on the stellar aspect of the simulation. In this formation scenario dark matter halos form independently first then merge to form the host galaxy. The host galaxy accretes smaller dark matter halos over different redshifts. Due to this formation structure, the inner tightly bound material is formed and accreted earlier than the outer regions (the halo) material. The halo of a galaxy forms out of the leftover gas and minor mergers of satellite galaxies. Applying this model to the Milky Way, this means that the central regions of the Galaxy (the bulge) would contain the oldest components.

Tumlinson (2010) show that stars with a given metallicity form over a wide range of redshifts. This is a result of the hierarchical nature of galaxy formation, chemical enrichment is different from one halo to the other depending on their star formation rate (SFR), which has some dependence on the halo mass. Depending on the location of the MP star in the Galaxy it may have formed at lower redshifts and won't be as useful for studying the conditions in the early Universe.

Figure 1.1 shows the distribution of star forming particles for stars with [Fe/H]< -1 as a function of radius from the center of a simulated galaxy (Salvadori et al. 2010). This study shows that the oldest star forming particles are concentrated in the innermost regions. Applying this to the Galaxy, the central regions are then an ideal place to hunt for the oldest Pop III survivors or those formed from their remnants. These stars would currently reside in the bulge region but this does not necessarily mean they formed in the bulge, that is to say they are in the bulge, but not of the bulge (Tumlinson 2010).

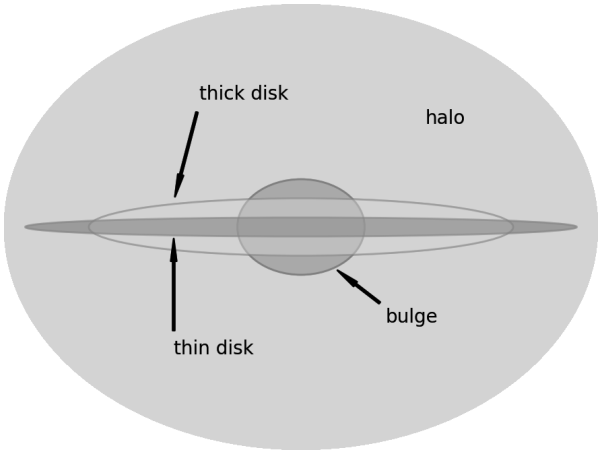

Figure 1.2: A schematic of the Milky Way galaxy to show the different components. The thin disk, thick disk, bulge and stellar halo.

Hence for studies concerning the early Universe, the tightly bound MP stars in the inner region of the Galaxy are our best candidates. Tumlinson (2010) show that the majority of stars with [Fe/H]$\leqslant 3$ in the central regions of the Galaxy are from $z > 10$ (~ 500 Myr after the Big Bang), and about $15 - 40\%$ are from $z > 15$.

1.5 The Galactic bulge

Stars in the Galaxy can be divided roughly into four stellar populations; the bulge, thick disk, thin disk and stellar halo. Figure 1.2 shows a schematic of the four components of the Galaxy. The different components form at different times during the Galaxy's formation process. The oldest components formed first in the central regions of the Galaxy (now in the bulge) (Tumlinson 2010). The bulge is considered the innermost region of the Galaxy, within 3.5 *kpc* from the Galactic center (located at $(l, b)^2 = (0, 0)$). Theories of the bulge's formation are divided into two main scenarios, either through early mergers during the Galaxy's formation or from disk instabilities (Bland-Hawthorn and Gerhard 2016). The merger scenario would form a spherical bulge, while disk instabilities would form a box-peanut (b/p) shaped structure (Ness et al. 2013, and references therein). Both features are observed in the Galaxy's bulge today.

The chemical enrichment of the bulge was rapid at early times due to a rapid SFR, as a result the bulge hosts both old MP stars and old moderately metal-rich stars (Freeman and Bland-Hawthorn 2002). Ness et al. (2013) suggest that the bulge might host as many as five separate populations, as shown in Figure 1.3. The two most MP populations in Figure 1.3 are attributed to the weak thick disk and the inner Galactic halo. The fraction of MP stars in the inner regions increases further away from the Galactic plane, making

[2] (l, b) refers to the Galactic coordinate system, Galactic longitude (l) and latitude (b).

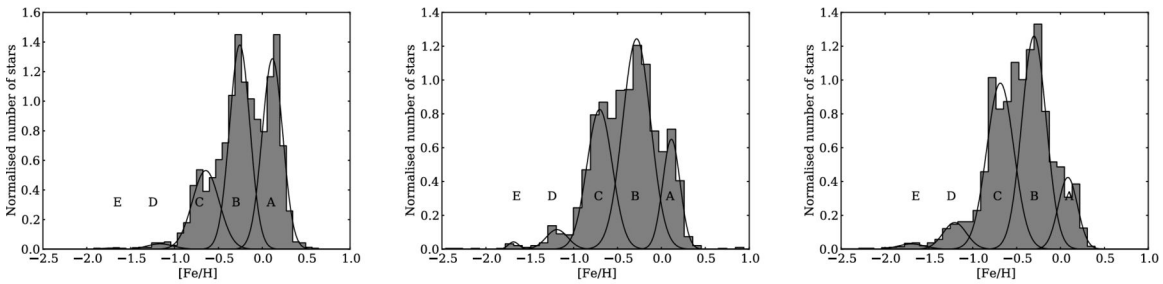

(a) $l \pm 15°, b = -5°$ (b) $l \pm 15°, b = -7.5°$ (c) $l \pm 15°, b = -10°$

Figure 1.3: Figure 11 from Ness et al. (2013). The figure shows the metallicity distribution function (MDF) for stars within a radius of $3.5\,kpc$ from the Galactic center at different Galactic latitudes $b = -5.0°, -7.5°, -10.0°$ and $l = \pm 15°$. The fraction of MP stars increases away from the Galactic plane.

the search for MP stars in the inner most regions of the Galaxy a challenging task. To find 10 MP stars in the bulge with [Fe/H]< -2, Ness et al. (2013) had to survey 10,000 stars. This shows how rare these stars are in the inner regions of the Galaxy.

1.6 Hunting MP stars

Over the past few decades several methods have been used to hunt MP stars in the Solar neighborhood and in the halo (Frebel and Norris 2015). More than 90% of MP stars discovered so far belong to the stellar halo (Yong et al. 2013; Roederer et al. 2014) and the rest from satellite dwarf galaxies (Frebel et al. 2010). This is due to two reasons, they are on average MP, and they are sparse with clear optical lines-of-sight towards the stars. These reasons make them preferable to search, rather than the inner regions. On the other hand the inner regions of the Galaxy are dense and on average metal-rich with clouds of dust blocking most of the optical lines-of-sight towards the stars, hence astronomers have avoided searching for MP stars in the bulge for years. MP stars in the bulge are extremely rare relative to more metal rich stars, the search for MP stars in the bulge is like looking for a needle in a haystack. Special techniques have to be used to improve the chances of finding such stars.

The EMBLA survey (Extremely Metal-poor BuLge stars with AAOmega[3]) utilizes the photometric data from the SkyMapper telescope to identify MP candidates (Keller et al. 2007). As shown in Howes et al. (2014), after the success of SkyMapper in identifying MP stars in the halo of the Galaxy using color-color plots, the hunt for MP stars in the bulge started by covering a $20° \times 20°$ field surrounding the Galactic center $(l, b) = (0, 0)$. Figure 1.4 shows the fields covered by SkyMapper and AAOmega. It is clearly visible from the plot that the central regions of the bulge have not been followed up by spectroscopy. The reddening effect due to dust clouds increases strongly towards the center of the Galactic plane, for this reason all stars followed up in high resolution lie more than 4° below or above the Galactic plane. A sample of 48 MP stars in the Galactic Center were observed at high

[3]AAOmega is a multi-object spectrograph on the AAT (Anglo-Australian Telescope).

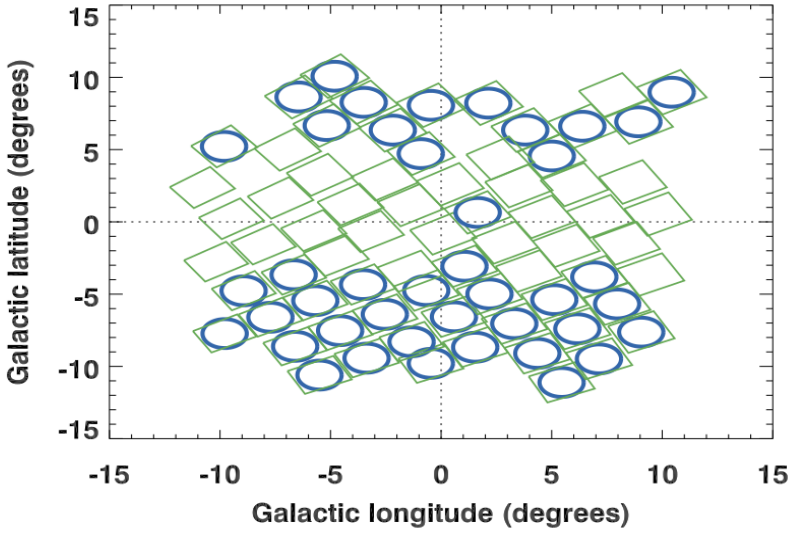

Figure 1.4: Figure 1 from Howes et al. (2016). The fields covered by SkyMapper photometry are shown as green boxes. The blue circles show regions followed up with spectroscopy by AAOmega.

resolution for this project as part of the EMBLA survey (for details on the observations see Howes et al. 2014, 2015, 2016).

1.7 Aim of this project

Were spinstars among the first stars in the Galaxy? This project aims to answer this question by studying the abundances of elements formed through the *s*-process in a sample of stars from the bulge of the Galaxy. The *s*-process elements of interest are strontium (Sr), yttrium (Y) and barium (Ba). Sr and Y are two light *s*-process elements, while Ba is a heavy one. Sr and Ba are detectable in nearly all MP stars discovered, even the most MP ones, making them an important tracer for the nucleosynthesis of heavy elements in the earliest times. In this work we are looking for one of the signatures of spinstars, which is an enhancement in the relative abundance of light (Sr and Y) to heavy (Ba) s-process elements.

We included europium (Eu) to the elements mentioned beforehand as it is a key tracer of the *r*-process. The interest in Eu comes from the subclasses of MP stars defined in Beers and Christlieb (2005). Using the relative abundance of [Ba/Eu], MP stars are classified as *r*, *s* or *r/s* rich stars. Eu is also of great interest to test for possible r-process production sites that explain the Eu abundances found.

The sample of stars in this work have two characteristics that make them some of the oldest stars discovered so far; they are MP and they reside within the inner regions of the Galaxy. By studying their chemical properties we aim to test the theory of spinstars being among the first stars of the Galaxy. We also compare our results to MP halo stars to see

if the formation site of the stars would result in different chemical properties.

1.8 Outline of the Thesis

The thesis is divided into 3 main chapters other than the Introduction. Chapter 2 covers the methodology followed to measure the abundances. Chapter 3 details our results, in Chapter 4 we discuss the results found and compare them with Galactic chemical evolution (GCE) models. Finally, Chapter 5 has the conclusions, answering the main question behind this thesis "Did spinstars exist in the early Universe?"

Chapter 2

Methodology

In this chapter we describe the methods used in this thesis. First we introduce Spectroscopy Made Easy (SME) (Valenti and Piskunov 1996; Piskunov and Valenti 2017), the software used in this work to determine the chemical abundances of the stars. Then we go through the methodology used for determining the stellar parameters of the stars and testing it on two benchmark MP stars. After that we describe how we measure the abundances for each element, first commenting on the line list selection, then the method followed for abundance determination, and then describing the method followed for calculating the uncertainties. Finally, the abundances for Sr, Y, Ba and Eu for 10 of the stars are compared to the corresponding values from Howes et al. (2016).

2.1 Spectroscopy Made Easy

As the main software used throughout this work, we include a brief description of SME. SME is a tool designed to automate the process of analyzing stellar spectra. It calculates synthetic spectra and fits them to observations. It can be used to determine stellar parameters, chemical abundances and spectral line data. SME consists of a solver and a graphical user interface (GUI) both written in `IDL`[1]. The solver uses external libraries written in `C++` and `Fortran`, as they are more efficient in handling computationally intensive calculations.

SME uses a chi-squared (χ^2) minimization algorithm to fit synthetic spectra to observations to find the stellar parameters or the abundances of specified elements. SME minimizes a weighted χ^2, where each pixel is weighted using the observed spectrum over pre-masked wavelength regions for both the line and the continuum regions. This weighting method gives more weight to points closer to the continuum compared to points closer to the core of the line, this method helps to decouple the influence of the continuum and line parameters (Piskunov and Valenti 2017). SME reads in an input file which contains the necessary information for the solver routine. The input data for SME consist of the following:

[1]Interactive Data Language, Harris Geospatial Solutions.

- The observed spectrum, wavelength segment/s to consider and a set of wavelength intervals specifying masks for regions to be used as lines/continuum.
- A set of model atmospheres, elemental abundances (Solar abundances from Grevesse et al. (2007)) and atomic data for absorption lines.
- Global parameters: fixed/initial values for the effective temperature (T_{eff}), surface gravity ($\log g$), metallicity ([Fe/H]), microturbulence (ξ) and macroturbulence (ζ).
- Flags for radial velocity and continuum scaling, fixed/initial values for radial velocity, projected rotational velocity at equator ($\mathrm{v}\sin i$).
- Free parameters: stellar parameters, elemental abundances or line data to solve for.

This input structure is prepared using the GUI. To efficiently use SME from the terminal, we use a wrapper written in `IDL` by Brian Thorsbro (PhD student at Lund Observatory at the time of this work), the script is described in Section 2.3. This wrapper prepares the input structure required by the SME solver routine, eliminating the need to interact with the GUI. It then sends the input file to SME's solver.

2.1.1 Model atmospheres and LTE

A stellar model atmosphere models the outer layers of a star from which the radiation escapes. A set of pre-calculated models is used by SME to calculate the synthetic spectra, these previously determined models describe the temperature, pressure and other physical properties of the gas as a function of the optical depth. As stellar atmospheres are complicated, with several physical quantities taking part in the overall state of the atmosphere, having a model that considers all these different quantities is computationally challenging. To overcome this problem astronomers often use assumptions that simplify the calculation of model atmospheres, commonly used assumptions to calculate model atmospheres are:

1. Hydrostatic equilibrium: This assumption assumes the gas in the atmosphere to be at rest, the force due to gravity is balanced by pressure forces. Large scale structure changes such as pulsations and mass loss are not accounted for. The atmosphere structure is independent of time.

2. Spherical, or plane parallel symmetry: Geometry considered when solving the radiative transfer equation and modeling atmospheres. In plane parallel geometry the thickness of the atmosphere is much smaller than the stellar radius, hence it can be treated as a flat plane.

3. Homogeneous: The physical quantities in the atmosphere vary with depth (radius) only, simplifying the problem from 3D to 1D.

4. Local thermodynamic equilibrium (LTE): For a small volume the gas is locally under thermodynamic equilibrium.

To calculate the synthetic spectra SME needs a set of model atmospheres from which it interpolates (extrapolates) a model atmosphere (set of T_{eff}, $\log g$ and [Fe/H]) that best fits the observations or to generate a model for a specific set of fixed parameters (Piskunov and Valenti 2017). We use MARCS 1D stellar model atmospheres (Gustafsson et al. 2008). These models apply the aforementioned assumptions, these assumptions seem over simplistic yet they are realistic enough to obtain a solid understanding of the stars being studied.

The equation of radiative transfer could be solved assuming either LTE or not, i.e. non-LTE (NLTE). We know that gas in stellar atmospheres is not under thermodynamic equilibrium, yet the assumption of LTE is a simplification to make the computation of model atmospheres much faster. LTE means that locally (on the scale of the optical depth), the gas is very close to thermodynamic equilibrium, the collisional interactions of atoms dominate over the radiative ones. This assumption means that the atmosphere of a star can be described using one temperature at a given optical depth. In this case the following laws apply to the gas, the velocity distribution of the atoms is described by a Maxwellian distribution, the population of different excited energy states is described by Boltzmann's law and the ionization equilibrium by Saha's law (see chapter 1 of Gray 2008, for detailed explaination of the three laws). All three laws depend mainly on the local temperature.

In the case of MP stars, the photospheres have low electron densities, which rise from the lack of metals (Asplund 2005). This causes the rate of collisions to decrease, leading to strong departures from LTE in some cases. Hence it must be noted that the use of NLTE models is important to consider for accurate abundance measurements in MP stars. In our case we use LTE abundances for the following reasons:

- NLTE abundance calculations for the heavy elements in this study are very computationally expensive.
- Observers often use pre-existing NLTE grids, no pre-existing grids exist for all the elements we are studying.

For now LTE abundances are the best we can do given they are interpreted correctly, keeping in mind that large deviations due to NLTE effects are possible. The sample of MP stars from François et al. (2007) was analyzed assuming LTE, Andrievsky et al. (2011) reanalyzed the sample measuring the abundances of Sr and Ba assuming NLTE. Andrievsky et al. (2011) conclude that the trends observed by François et al. (2007) in the [Sr/Ba] vs. [Ba/H]([Fe/H]) plots using LTE abundances are still present with the same degree in their measurements when correcting for NLTE, that is an increase in Sr with decreasing Ba. They also mention that the scatter of the Sr abundances between individual stars at the lowest metallicities is even stronger than in the LTE case. From this we see that the use of LTE for the abundances is satisfactory for the goals of this study, as the trends in the abundances are what concerns us the most, rather than the absolute values.

2.2 Stellar parameters

The stellar parameters used in this work were measured by Dr. Louise Howes using SMH (Spectroscopy Made Hard (Casey 2014). Table A.1 lists the stellar parameters measured with uncertainties. In order to check if using the different softwares/methods would cause any biases or introduce extra errors in the measurements, I tested SME on two MP benchmark stars HD122563 and HD140283 using the publicly available UVES/VLT spectra from the UVES Paranal Observatory Project database (Bagnulo et al. 2003), the stellar parameters for which are taken from Jofré et al. (2014) and Heiter et al. (2015a). Here we describe the method I followed to find the stellar parameters in SME for the two benchmark stars and compare them to those found using SMH by Louise (following the same method) and to the literature values.

2.2.1 Effective temperature

We use the wings of the hydrogen Balmer alpha line (H_α $\lambda = 6562.8$Å) and hydrogen Balmer beta line (H_β $\lambda = 4861.3$Å) to fit for the effective temperature. Hydrogen is the most abundant element in stellar atmospheres and the few spectral lines that it produces are strongly present in stars of all spectral types. The strength of these lines are very sensitive to changes in the effective temperature, while they are weakly affected by the surface gravity. This is true for stars with effective temperatures below about $8000K$ (Gray 2008). This makes them a key feature for determining the effective temperature of stellar atmospheres. Figure 2.1 shows an example of how the strength of the H_β line changes with temperature, the wings are stronger for higher effective temperatures.

For determining the effective temperature (T_{eff}), the same method is used in both SME and SMH. The steps followed are:

1. The literature parameters are used as initial values. This step does not affect the values SME or SMH converge to, it mainly helps the solver to converge faster.

2. We then solve for T_{eff} only, with the other parameters fixed. Each of the hydrogen Balmer lines are solved for separately.

3. The final T_{eff} is then the average of the values from both the H_α and H_β lines.

We then move on to calculate the other parameters ($\log g$, [Fe/H] and ξ) as explained in the next section.

2.2.2 Surface gravity, metallicity & microturbulence

The surface gravity ($\log g$), metallicity ([Fe/H]) and microturbulence (ξ) are found using a combination of neutral and singly ionized iron lines (FeI & FeII). First we discuss how SME is used to determine these three parameters, then we describe the method followed when using SMH.

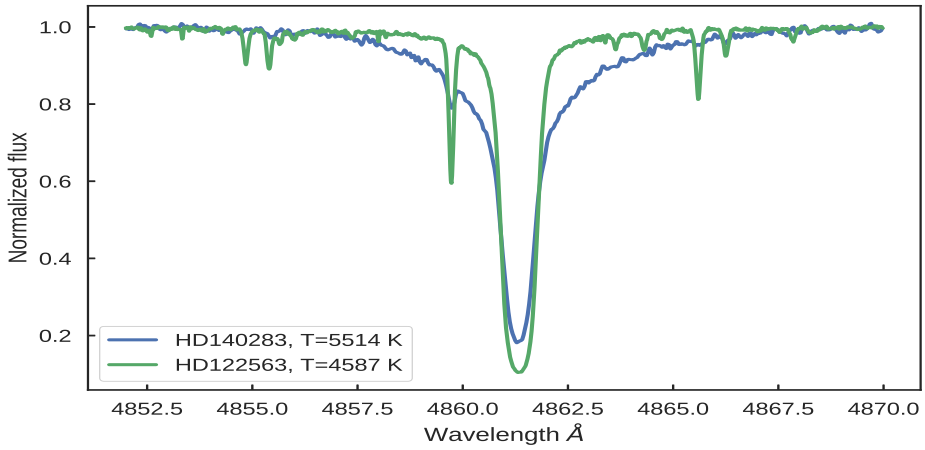

Figure 2.1: A plot of the H_β line in the two benchmark MP stars HD122563 (giant) and HD140283 (subgiant). The plot shows how the wings of the line are affected by the difference in temperature, the wings being stronger for the higher effective temperature, values from Heiter et al. (2015a).

SME

In SME, $\log g$, [Fe/H] and ξ are determined simultaneously by specifying spectral regions that contain a group of FeI and FeII lines. SME arrives to the set of parameters that best fit the observed spectrum by fitting a synthetic spectrum to the observations. The macroturbulence is set as a free parameter and $v \sin i$ is fixed to zero during this process as SME attempts to fit the abundances of Fe for the metallicity determination.

After SME converges to a set of parameters, the effective temperature is then recalculated using the new $\log g$, [Fe/H] and ξ. We iterate between the calculation of T_{eff} and the steps mentioned here until the values converge. The following convergence criteria is followed, the change in T_{eff} is smaller than 50K and the change in $\log g$ and [Fe/H] is around 0.05 dex between two iterations.

SMH

In SMH the surface gravity is found by the ionization balance of the abundances from FeI and FeII lines, this is achieved by minimizing the difference between the abundance of FeI and FeII lines. NLTE corrections for Fe are included, which affects the abundances of FeI lines. The surface gravity is then found by setting the difference between the abundances of FeI and FeII to the NLTE correction value.

The metallicity is then set equal to the mean abundance of FeII, as NLTE does not affect the abundances from FeII lines as much compared to FeI lines.

The microturbulence is found by minimizing the trend between FeI line abundances and the reduced equivalent width. The reduced equivalent width is the equivalent width[2]

[2]EQW: The width of a column of 100% absorption with the same area as the spectral line.

Table 2.1: Comparison between stellar parameters calculated for two MP benchmark stars HD122563 (giant) and HD140283 (subgiant). To validate our methodology we tested it on both these stars and compared the parameters found to those found by Louise using SMH and to values from the literature.

		SME	SMH	Literature*
HD122563	T_{eff}(K)	4605	4635(±160)	4587(±60)
	$\log g$(dex)	1.2	1.15(±0.13)	1.61(±0.07)
	[Fe/H](dex)	-2.6	-2.67(±0.06)	-2.64(±0.22)
	ξ(km/s)	1.9	1.98(±0.20)	1.92(±0.11)
HD140283	T_{eff}(K)	5510	5696(±160)	5514(±120)
	$\log g$(dex)	3.25	3.55(±0.13)	3.57(±0.12)
	[Fe/H](dex)	-2.90	-2.52(±0.05)	-2.36(±0.10)
	ξ(km/s)	1.00	1.00(±0.20)	1.56(±0.20)

*Literature values from Jofré et al. (2014); Heiter et al. (2015a)

of the line divided by the wavelength.

Once the new set of $\log g$, [Fe/H] and ξ are calculated, the effective temperature is recalculated using the new parameters. Similar to the method followed in SME, we iterate between determining T_{eff} and the other parameters ($\log g$, [Fe/H] and ξ) until the values converge following the same criteria.

2.2.3 Comparison with literature values

The comparison between SME and SMH helps identify any systematic errors introduced due to the different softwares. In order to check for the credibility of the derived parameters, we compare our measurements (using SME and SMH) to values adopted in the literature for the two benchmark stars. We did not calculate the uncertainties in the parameters using SME. We consider the values to be in good agreement if the difference between the values is within $1\,\sigma$.

The literature values are from the Gaia FGK benchmark stars sample (Jofré et al. 2014; Heiter et al. 2015a). The effective temperature and surface gravity are measured from interferometry (for details see Heiter et al. 2015a). The metallicity is calculated as the mean of the line by line abundance of FeI (for details see Jofré et al. 2014). Table 2.1 shows the results from SME compared to those from SMH and the literature. We briefly comment on the results of this comparison.

Effective temperature

The effective temperature derived using SME for the giant star HD122563 is in good agreement with the value found using SMH and the literature value. Our value from SME is within $1\,\sigma$ from SMH and the literature values, where the difference is $30K$ and $18K$ respectively. For the subgiant star HD140283 SME and SMH values do not agree as well with a difference of $(186K)$, though SME is in very good agreement with the literature value, with a difference of $(\sim 4K)$.

Surface gravity

For HD122563, the SME value agrees very well with SMH, with a difference of 0.05. The value from SME, similar to SMH, is far from the literature value with a difference of 0.41. What concerns us the most is the agreement between both SME and SMH. Amarsi et al. (2016) predict that for HD 122563 the literature parallax-based $\log g$ is over estimated, as this star needs strong NLTE corrections. They measure a $\log g$ value of 1.1 for this star, the measurements from SME and SMH agree well with Amarsi et al. (2016)'s measurement.

For HD140283 the surface gravity from SME does not compare well to the values from the literature and SMH. SME underestimates it with a difference of $\log g \sim 0.3$ from both the literature and SMH.

Metallicity

The metallicity estimated by SME for HD122563 is in very good agreement with the literature and SMH with a difference of 0.04 and 0.07 dex respectively. For HD140283, similar to the case with $\log g$, the metallicity from SME is underestimated compared to the literature and SMH with a difference of 0.6 and 0.4 dex respectively. SME does not include NLTE effects, which would contribute to the differences measured. Different atmospheric models would contribute to this difference as well.

As the stars in our sample are all giants, with stellar parameters different from HD140283, this offset between SME and SMH for this star perhaps matters less. Our method and models are more compatible with giant stars. As seen from Table 2.1, for HD122563 SME and SMH agree really well on all the derived stellar parameters (T_{eff}, $\log g$ and [Fe/H]). From this we find that using the stellar parameters derived using SMH by Louise for our sample of stars is justified and should not introduce any unexpected errors in the measured abundances.

2.3 Elemental abundances

To determine the chemical abundance of a star we need the following: a line list with the atomic data for the spectral lines, software to measure the abundances, a model atmosphere, and high resolution spectrum with a high signal to noise ratio (SNR). Here we

shortly describe the line list used in this work and the method followed in SME to measure the abundances and their uncertainties. In this work we measure the abundances under the assumption of LTE. The effects from NLTE will be systematic for all measurements, hence any trends in the abundances plots should be the same if we solve assuming LTE or not, as discussed in Section 2.1.1.

2.3.1 Line list

The line list containing the atomic data for the lines used is obtained from VALD[3]. The line list contains the atomic transition parameters needed for the chemical abundance calculation. The following information is available for each line:

- The species of the element and ionization state,
- The wavelength of the spectral line,
- The excitation potential of the lower energy level, and
- The oscillator strength ($\log gf$).

The line list used includes isotopic shifts for Ba and Eu (included in VALD). Table B.1 shows the atomic data. The selected lines were checked to be free of blends with other spectral lines, for more details on the line selection see Howes et al. (2016) and the Gaia-ESO line list (Heiter et al. 2015b).

2.3.2 Abundance measurement

The spectra of our stars were reduced and normalized following the method described in (Howes et al. 2016), as SME handles only reduced spectra with a limited capacity to normalize. An `IDL` script (hereafter "SME wrapper") is used to efficiently use SME by calling it the solver routine from the terminal, without the need for the GUI supplied with the tool. This script prepares the input file required by SME's solver, then sends the file to SME for calculations.

SME wrapper

The wrapper reads in a configuration file from which it prepares the input file for SME. The configuration file is divided into 8 main sections containing basic information needed by SME, we list the sections here with the information included in each.

essential: This section contains the paths for the following files: observed spectrum, line/continuum masks, wavelength segment/s, line list and output file for SME.

[3] http://vald.astro.uu.se/

glob_par: This section contains the initial/fixed values for T_{eff}, $\log g$, metallicity [Fe/H], ξ, ζ, $\mathrm{v}\sin i$, v_{rad} and SNR.

sme: This section includes a flag for SME to handle the radial velocity and continuum scale, it also contains the resolution of the observed spectrum.

glob_free, ab_free, gf_free & vw_free: These sections contain the free parameters for SME to solve for. This could be stellar parameters, abundances, $\log gf$ or van der Waals damping values respectively.

abund: This section names the base abundances to be used by SME, in our case we use the Solar abundances from Grevesse et al. (2007).

Abundance script

For the abundance determination I wrote a `Python` script (hereafter "abundance script") that writes the configuration file, the abundance script then calls `IDL` which runs the SME solver routine using the configuration file. The abundance script caries out the following tasks:

- Set the boundaries of the segment to work on and calculate the SNR for it following the method described in Stoehr et al. (2008). If the SNR is less than 10 the spectral line is discarded.
- Find the wavelength region to assign as line mask (lmask), this is done by scanning a 0.7Å region on both sides of the spectral line's center. The script searches for the nearest local maxima. If there are isotopic shifts for the spectral line, the script sets a condition to make sure the line mask includes all local maxima within the isotopic shifts range.
- Assign regions as continuum masks (cmask), this is done by selecting all spectral points within 5Å from the boundaries of lmask with intensities ($\mathrm{I} > signal - 0.75 \times noise$). I tested different values for different SNR's, the value of 0.75 worked best for all spectral regions. The script then selects regions wider than 0.1Å and saves them as continuum mask regions .
- Measure the strength of the spectral line, if the core of the line is less than 3σ from the signal level the line is discarded. This step is visually inspected in case of false positives. In some stars with high SNR's the lines are strong enough to be reliably measured, even if the core is less than 3σ away from the continuum level.
- Write out the lmask boundaries and line center, boundaries for the cmask regions, and the segment limits to three separate files.
- Write out the configuration file. The script sets the stellar parameters, the paths to the files created in the previous step, the paths to the spectrum and line list files, and which element to solve for.

The SME wrapper reads the configuration file to create SME's input file, then passes it to the solver in `IDL` to calculate the abundance of the specified element. I set the macroturbulence free during the abundance calculation and $v \sin i$=0. Once SME converges to a value, the abundance script saves the value found and plots the observed spectrum with the fitted synthetic spectrum for visual inspection. In the case of having several lines for the element specified, the abundance script feeds SME each line separately. The final abundance calculated for each star by the abundance script is the mean of the individual lines.

SME can treat the continuum scale differently depending on the flag assigned in the input structure. The default case when a continuum mask is selected SME uses the selected region to renormalize the spectrum. This method works best for spectra with high SNR, unlike the SNR for our stars which is somewhat lower. Hence we follow a different method to place the continuum for each segment. After the cmask regions are selected, the mean of the flux values from these regions is used as the continuum level. The abundance script then renormalizes the spectrum using this new continuum level, SME then treats the spectrum as normalized by placing the continuum at 1. In some cases for segments with low SNR (< 25), the continuum level needs small manual adjustments (on the scale of 0.5%) by visually inspecting the output plot of the observation with the synthetic spectrum.

2.3.3 Uncertainty measurements

The uncertainties in the stellar parameters are used to find the error in abundances from each parameter on its own. The abundance from each line is recalculated using the upper and lower limits of each parameter separately. The following steps are followed to measure the uncertainty for each element per star:

1. Solve for the abundance using the upper limit for one parameter (T_{eff}, $\log g$, [Fe/H] or ξ), the other parameters are fixed to their true value. This gives a new abundance per line, X_u is the mean of the abundances found.

2. Solve for the abundance using the lower limit for the same parameter with the other parameters unchanged. This gives a new abundance per line, X_l is the mean of the abundances found.

3. $\sigma_u = |X - X_u|$, and $\sigma_l = |X - X_l|$ are the difference in the abundance due to the uncertainty in the selected parameter, where X is the abundance found using the stellar parameters.

4. The uncertainty in the abundance due to the error in the parameter is $\sigma_{param} = \frac{\sigma_u + \sigma_l}{2}$.

5. Repeat 1-4 for the other three parameters.

The overall error in abundance is calculated by summing the individual errors in quadrature as shown in Equation 2.1. This method does not take into account any correlations between the stellar parameters, which is most likely the case. The full error matrix for the stellar

parameters is not available to us to account for the error correlations. σ_{mean} in Equation 2.1 is the standard error of the mean abundance calculated using Equation 2.2, where N is the number of lines for each element and σ is the standard deviation of the individual line abundances. The uncertainties in the stellar parameters take into account systematic errors due to the method used (see Howes et al. 2015, for details).

$$\sigma_{total} = \sqrt{\sigma^2_{mean} + \sigma^2_{Teff} + \sigma^2_{logg} + \sigma^2_{[Fe/H]} + \sigma^2_{\xi}} \tag{2.1}$$

$$\sigma_{mean} = \frac{\sigma}{\sqrt{N}} \tag{2.2}$$

2.4 Earlier studies of 10 MP bulge stars

Howes et al. (2016) carried out a detailed analysis of 10 of the stars in this sample measuring the abundances of 22 elements including Sr, Y, Ba and Eu. Sr and Ba are measured for all 10 stars while Y and Eu are measured for 9 and 7 stars respectively. In this section we compare the abundances measured for these elements in this study to the values reported by Howes et al. (2016). In Howes et al. (2016) the stellar parameters used are the same as this study, the main difference is the code used to measure the abundances. The lines used to determine the abundances of Sr, Ba and Y are the same for both studies, while for Eu we include two extra lines at 3819.6 and 3907.12 Å.

The abundances for Ba from both studies are in good agreement, this is less true for the other elements. In Figure 2.2c, the abundances for Ba from this study are plotted against the abundances from Howes et al. (2016), we plot a 1:1 relation line and the best fit to the data points. It is clear from the plot that for Ba both studies agree really well, with an average offset of $\sim$0.05 dex. This agreement between both studies is mainly due to both studies using the same technique of fitting synthetic spectra to measure the abundances of Ba and using the same spectral lines with the same atomic data.

The method followed for calculating the abundances of Sr, Y and Eu is different between both studies. We use the method of fitting synthetic spectra to the observations in order to measure the abundances. In Howes et al. (2016) they employ the method of measuring the equivalent width by fitting a line profile to the spectral line, the continuum placement from this technique is different from our method, most likely introducing the systematic differences seen in Figures 2.2a,b,d.

For Sr the abundances from this study are on average higher than the values from Howes et al. (2016), with an average offset of $\sim$ 0.17 dex. We can attribute this offset mainly to the different methods as mentioned before and to using different atomic data. In this study we use the excitation energies and $\log gf$ values retrieved from VALD while in Howes et al. (2016) the used values are different, the values from VALD are higher than those used in Howes et al. (2016) for both spectral lines. The atomic data for Y is the same in both studies yet the abundances from this study are on average higher, the average offset is $\sim$0.19 dex. Similar to Sr and Y, Eu measurements from this work are on average higher than Howes et al. (2016) by $\sim$ 0.17 dex. Other than the different methods, the

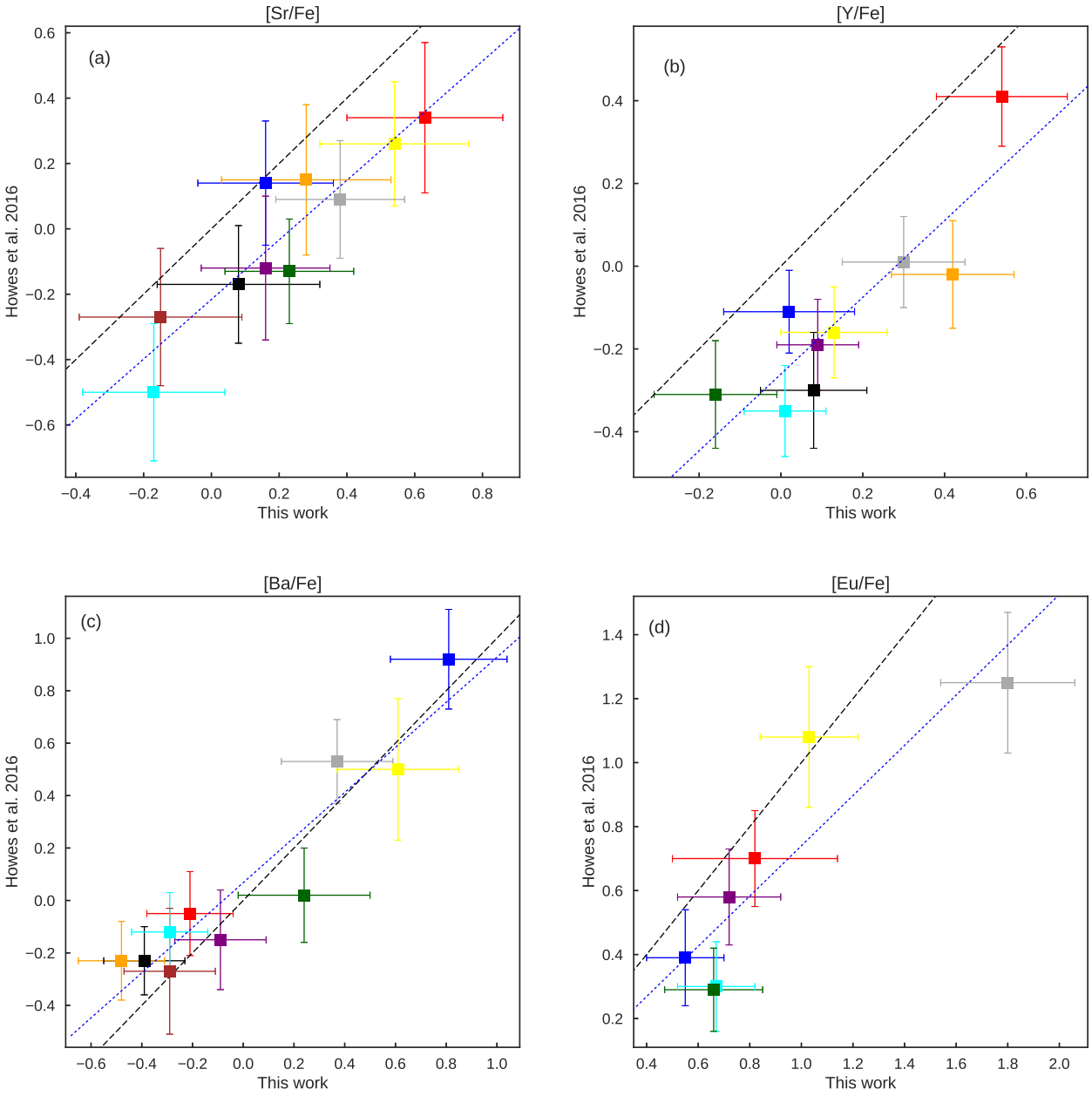

Figure 2.2: In these plots we show a comparison between the abundances of Sr, Y, Ba and Eu from this study and Howes et al. (2016). Each star is represented by the same color in each plot. The black dashed line shows a 1:1 relation and the blue dotted line is the best fit to the data points. The Sr abundances from this study are systematically higher than those reported in Howes et al. (2016), the same is seen for Y and Eu. The average offset is $\sim 0.17, 0.19, 0.17$ dex for Sr, Y and Eu respectively. The abundances for Ba are in good agreement between both studies, with an average offeset of $\sim$ 0.05 dex. See the text for discussion.

atomic data for the Eu lines used is different. We include isotopic shifts for the Eu lines, this is not included in Howes et al. (2016) which leads to different measurements.

Both studies have measured Sr and Ba in all the stars, from Howes et al. (2016) one star had no Y and Eu measurements and two other stars had no Eu measurements. Howes et al. (2016) did not report a measurement for Y and Eu for star SMSS J182948.50-341053.9, here we were able to measure one line for each element in this star. For the other two stars with no Eu measurements from Howes et al. (2016), we were not able to measure Eu in them as well.

In conclusion, the abundances for Ba from both studies agree well due to using the same measuring techniques. This is not the case for the other three elements Sr, Y and Eu, where this study is on average higher with an offset of about 0.17 dex. This difference is traced back mainly to the different measurement techniques (continuum treatment), using different atomic data in the case of Sr and Eu, and using different lines for Eu. This offset must be considered in the case of directly comparing both studies. The methods followed in this work and in Howes et al. (2016) are both valid, but in our case we use better atomic data for these elements. We suggest that these results are more reliable.

Chapter 3

Results

3.1 Abundances

The abundances measured in this work are plotted against a sample of MP halo stars from François et al. (2007) (FRA07), Barklem et al. (2005) (BAR05) and Roederer et al. (2014) (ROE14b). The samples from BAR05 and ROE14b are two of the largest MP halo samples that are homogeneously analyzed (each sample separately). ROE14b contains 184 MP halo stars that are giants and subgiants. BAR05 is a sample of 186 stars analyzed using SME, the stars have high resolution (R$\sim$20,000) spectra with SNRs comparable to that of the stars in this work. Comparing our results to BAR05's halo sample eliminates any errors introduced due to the analysis software SME.

The sample from FRA07 is part of the ESO Large Programme "First Stars", this sample contains 30 stars with high resolution (R=47,000) and high SNR. We include the FRA07 sample for the reasons mentioned at the end of Section 2.1.1, about NLTE vs. LTE abundances. In their analysis they see an increase of light s-process elements (Sr, Y and Zr) compared to heavy ones (Ba) with decreasing metallicity. They conclude that some unknown process must be responsible for 90% of the production of these light n-capture elements in the early Universe along with the r-process.

First we list our final abundances in Table 3.1, the final abundances shown in the table are the mean value from all the measured lines per element. The results for each element are discussed afterwards. In this chapter we list our results, focusing mainly on the comparison with MP stars from the halo. We discuss the trends and behavior of the elements relative abundances to both Fe and H versus the stars' metallicity ([Fe/H]). We postpone the discussion of the element-element comparison to the next chapter along with the comparison to the yields from spinstar models.

I was able to measure Sr in 44 stars, the wavelength coverage of the remaining four stars' spectrum did not cover the Sr lines region. For Ba, I was able to measure it in 46 of the stars, the SNR of SMSS J175510.50-412812.1 was too low to reliably measure the Ba lines (or any other element) and for SMSS J181609.62-333218.7 there are no detectable Ba lines. I managed to measure Y and Eu in 41 and 31 stars respectively, the missing

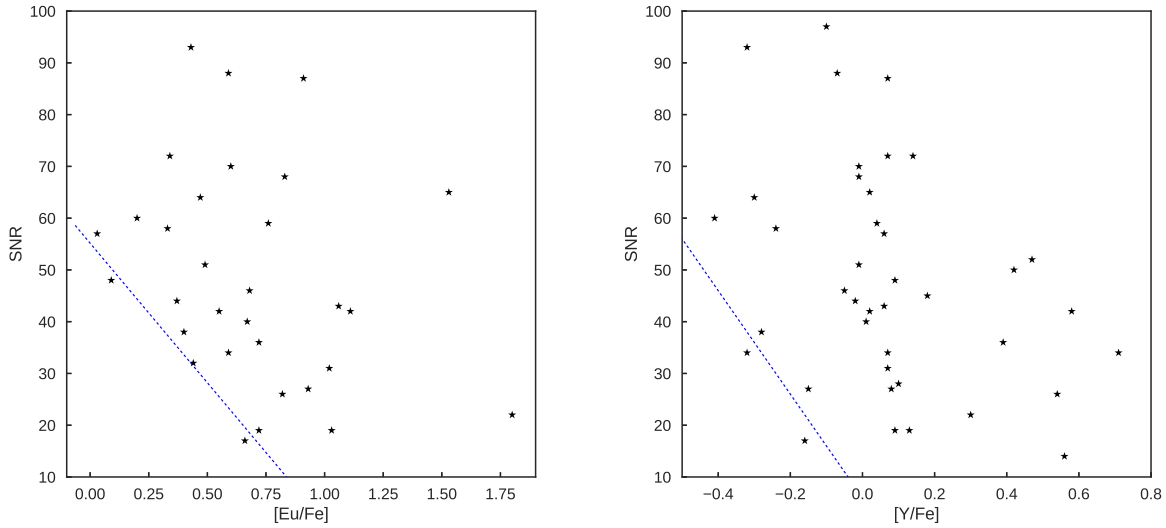

Figure 3.1: This figure shows the relation between the SNR and both the [Eu/Fe] and [Y/Fe] abundance measured for each star. The dashed blue line is the best linear fit to the few stars at the lower left end of the sample, it marks the clear dependence of the Eu and Y lower limit detection on the SNR.

measurements for these two elements are mainly due to low SNR values or weak lines.

I find a clear relation between the SNR of a star and the ability to measure an abundance for both Y and Eu. This dependence shows that higher SNR values are needed to better study these elements. Figure 3.1 shows these relations, where we plot the SNR vs. [Eu/Fe] (to the left) and SNR vs. [Y/Fe] (to the right) . There is a clear lower boundary to what [Eu/Fe]([Y/Fe]) values I can measure depending on the SNR of the star. The dashed blue line in each plot is the best linear fit to the 5(4) stars for Eu(Y) at the lower left edge of the sample. The fact that there are no outliers in the bottom left corner (under the dashed blue line), validates our line selection criteria. Hence we can say that our measurements are reliable.

Table 3.1: Mean abundances normalized to Solar values from Grevesse et al. (2007). The final abundances shown in the table here are the mean value from all measured lines per element. The uncertainty for each element is calculated using Equation 2.1.

Star name (SMSS)	[Fe/H]	$\sigma_{[Fe/H]}$	[Sr/Fe]	σ_{Sr}	[Y/Fe]	σ_{Y}	[Ba/Fe]	σ_{Ba}	[Eu/Fe]	σ_{Eu}
J182637.10-342924.2	-1.97	0.08	0.16	0.2	0.02	0.16	0.81	0.23	0.55	0.15
J182948.48-341053.9	-2.47	0.11	-0.15	0.24	0.39	0.16	-0.29	0.18	0.72	0.26
J182600.10-332531.0	-2.53	0.08	0.08	0.24	0.08	0.13	-0.39	0.16	-	-
J182601.24-332358.3	-2.83	0.11	0.63	0.23	0.54	0.16	-0.21	0.17	0.82	0.32
J182753.81-334607.7	-2.31	0.06	0.16	0.19	0.09	0.1	-0.09	0.18	0.72	0.2
J183000.40-333919.3	-2.63	0.07	-0.17	0.21	0.01	0.1	-0.29	0.15	0.67	0.15
J182922.48-335559.4	-2.77	0.08	0.28	0.25	0.42	0.15	-0.48	0.17	-	-
J182930.47-335958.3	-1.97	0.12	0.23	0.19	-0.16	0.15	0.24	0.26	0.66	0.19
J183225.29-334938.4	-1.74	0.09	0.54	0.22	0.13	0.13	0.61	0.24	1.03	0.19

Table 3.1 Continued:

Star name (SMSS)	[Fe/H]	$\sigma_{[Fe/H]}$	[Sr/Fe]	σ_{Sr}	[Y/Fe]	σ_{Y}	[Ba/Fe]	σ_{Ba}	[Eu/Fe]	σ_{Eu}
J183128.71-341018.4	-1.83	0.1	0.38	0.19	0.3	0.15	0.37	0.22	1.8	0.26
J182153.85-341018.8	-2.51	0.07	-	-	-0.51	0.12	-0.44	0.19	-	-
J183617.33-270005.3	-2.8	0.1	-	-	0.07	0.13	0.35	0.22	-	-
J175510.50-412812.1	-2.36	0.31	-	-	-	-	-	-	-	-
J175652.43-413612.8	-2.39	0.13	-	-	-	-	-0.13	0.21	-	-
J173823.38-145701.1	-3.36	0.1	0.23	0.25	0.07	0.12	-0.19	0.18	0.34	0.12
J182048.26-273329.2	-3.48	0.09	-0.45	0.23	-	-	-0.18	0.16	-	-
J183744.90-280831.1	-2.92	0.07	-0.12	0.26	0.06	0.14	-0.46	0.16	0.03	0.11
J183647.89-274333.1	-2.48	0.06	0.47	0.19	0.06	0.12	0.1	0.22	1.06	0.16
J183812.72-270746.3	-3.22	0.08	-0.94	0.22	-	-	-1.41	0.17	-	-
J183719.09-262725.0	-3.18	0.07	0.39	0.24	0.71	0.24	-0.73	0.16	-	-
J184201.19-302159.6	-2.84	0.07	-0.07	0.26	0.04	0.14	-0.09	0.16	0.76	0.12
J184656.07-292351.5	-2.76	0.07	-0.15	0.26	-0.3	0.13	-0.53	0.18	0.47	0.22
J181406.68-313106.1	-2.82	0.06	-1.58	0.18	-	-	-0.88	0.14	-	-
J181317.69-343801.9	-2.28	0.06	0.16	0.21	-0.01	0.13	0.19	0.21	0.49	0.2
J181219.68-343726.4	-2.5	0.07	0.1	0.23	-0.05	0.13	0.17	0.22	0.68	0.16
J181609.62-333218.7	-3.94	0.16	-0.85	0.21	-	-	-	-	-	-
J181634.60-340342.5	-2.46	0.06	-0.17	0.25	-0.41	0.13	-0.3	0.2	0.2	0.16
J175544.54-392700.9	-2.65	0.07	0.07	0.24	0.09	0.15	-0.16	0.2	0.09	0.09
J175455.52-380339.3	-3.36	0.14	0.69	0.25	0.14	0.21	-0.73	0.21	-	-
J175746.58-384750.0	-2.81	0.1	0.05	0.3	0.07	0.15	0.08	0.18	1.02	0.2
J181736.59-391303.3	-2.59	0.09	0.02	0.22	-0.24	0.14	-0.33	0.2	0.33	0.11
J181505.16-385514.9	-3.29	0.1	-0.11	0.24	0.18	0.17	-0.08	0.17	-	-
J181921.64-381429.0	-2.72	0.07	-0.11	0.25	-0.01	0.12	-0.07	0.18	0.83	0.16
J175722.68-411731.8	-2.88	0.07	-0.15	0.25	-0.07	0.14	-0.37	0.16	0.59	0.14
J175021.86-414627.1	-2.6	0.07	-0.07	0.25	-0.32	0.15	-0.26	0.17	0.43	0.17
J175636.59-403545.9	-3.21	0.13	0.79	0.25	0.47	0.18	-1.25	0.21	-	-
J175433.19-411048.9	-3.26	0.11	-0.75	0.23	-0.1	0.16	-0.71	0.2	-	-
J181815.99-242253.2	-2.72	0.07	-0.1	0.32	-	-	-0.28	0.19	0.44	0.12
J170817.27-293928.9	-2.3	0.07	0.27	0.2	-0.15	0.11	-0.08	0.22	0.93	0.28
J165605.96-342646.4	-2.48	0.09	0.13	0.2	-0.32	0.12	-0.17	0.23	0.59	0.31
J181722.18-335209.4	-2.52	0.08	0.11	0.23	-0.28	0.13	-0.18	0.23	0.4	0.18
J181946.17-340737.3	-2.25	0.06	0.35	0.2	0.07	0.13	0.04	0.2	0.91	0.15
J182051.46-340733.3	-2.38	0.07	0.27	0.2	0.02	0.13	0.25	0.23	1.53	0.22
J175140.30-382955.6	-2.34	0.06	0.36	0.19	-0.01	0.12	-0.28	0.2	0.6	0.14
J175633.89-414628.6	-2.46	0.11	0.03	0.27	0.1	0.17	0.26	0.23	-	-
J175610.36-414650.8	-2.34	0.09	0.38	0.22	0.58	0.13	0.5	0.18	1.11	0.15
J175400.31-402621.7	-2.25	0.13	0.25	0.26	0.56	0.16	0.13	0.21	-	-
J175432.75-410749.6	-2.4	0.08	0.31	0.22	-0.02	0.15	0.26	0.23	0.37	0.14

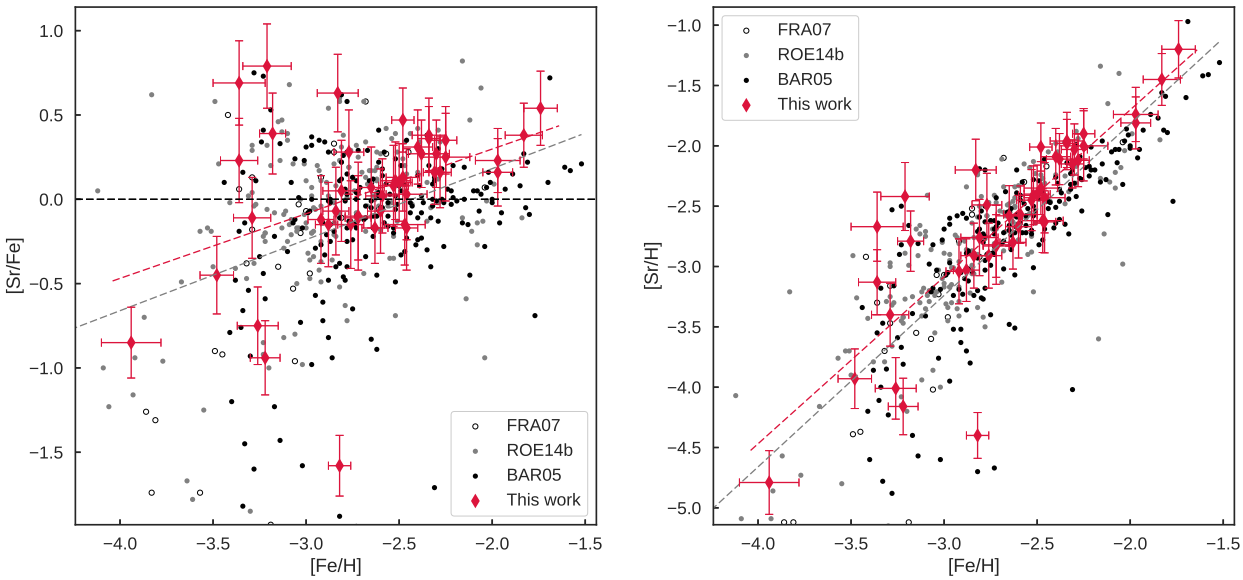

Figure 3.2: The red diamonds show the measured values from this work with uncertainties. The black circles are taken from Barklem et al. (2005), the white circles from François et al. (2007) and the gray circles from Roederer et al. (2014). The dashed line shows the Solar value. The stars from this study show a scattered behavior as seen for the halo stars, pointing towards similar chemical enrichment processes taking place in both regions of the Galaxy.

3.2 Sr

The abundances measured for Sr are shown in Figure 3.2. The scatter between the individual stars increases with decreasing metallicity with an overall slightly decreasing trend, similar to what is observed for MP stars in the halo. This wide scatter at the lowest metallicities could be due to the early Galaxy not being chemically mixed; elements blown out to the ISM from dying stars only enrich the local space around them and it would take longer for the ISM to mix homogeneously throughout the Galaxy (Karlsson et al. 2013). Sr is predominantly an s-process element, we do not expect the ISM to be enriched with Sr for a few hundred *Myrs* at least, until a time equivalent to [Fe/H]~ -2 (Sneden et al. 2008). This metallicity can only be considered as an indicator of age, however we do not know of a clear age-metallicity relation through the Galaxy. We expect our stars to be old and would have formed at a time before any AGB contribution to the ISM took place, meaning that any s-process elements would have to be produced in a different site.

The relative Sr abundances for stars with [Fe/H]$\geqslant -2.5$ are higher than that of the Sun. For stars with lower metallicities the scatter is extremely wide covering a range of ~ 2 dex, similar to the halo stars. This agreement between our stars and the stars from the halo points towards similar chemical enrichment processes taking place in the bulge and halo. Intuitively we would expect the chemical enrichment in the different regions of the

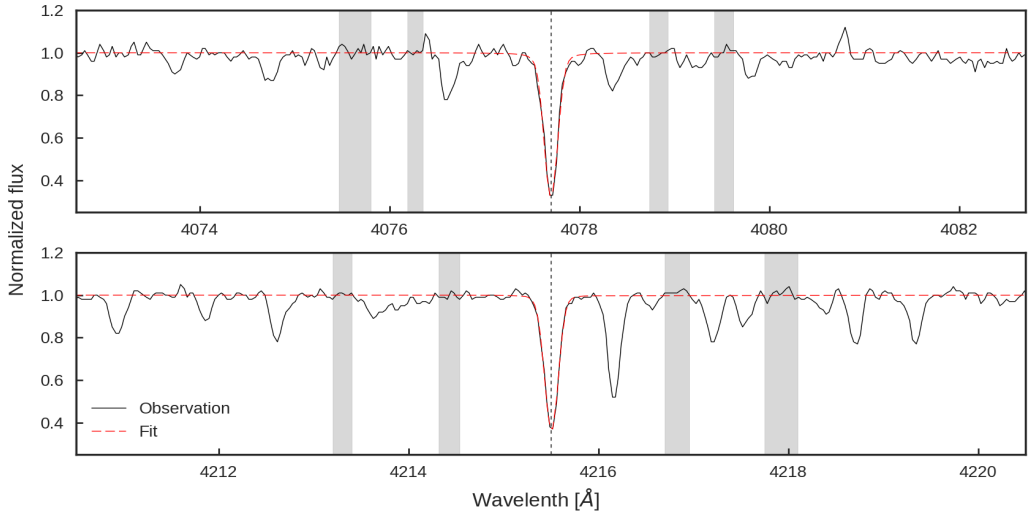

Figure 3.3: The figure shows an example for the fit of the two Sr lines that we use for the abundance measurements, the observed spectrum is shown in black and the fitted spectrum in red. The gray regions mark the continuum masks. This fit is for star SMSS J175021.86-414627.1 with a SNR of 93 and [Sr/Fe]= −0.7.

Galaxy to differ depending on the SFR. I find one star with extremely low [Sr/Fe]= −1.58, with only a few halo stars at the same level. I discuss this star's behavior in Section 4.1.4.

The main result from Figure 3.2 is that for Sr, MP bulge and halo stars show similar behavior. The stars from our sample are on average 0.15dex higher than the halo sample, which is at the level of being indistinguishable from systematic offsets.

In Figure 3.3, we show an example for the synthetic spectrum fitted to the spectral region around the two Sr lines at 4077Å and 4215Å. To get the best fit we try to make the continuum level agree with the observation within $\sim$ 5Å on both sides of the line. These two resonance lines are quite strong in most of the stars, the equivalent widths are around $150 - 200\,m$Å. However, they are the only measurable Sr lines at these metallicities, and are widely used in MP literature.

3.3 Y

Y is one of the light s-process elements, it belongs to the first s-process peak, like Sr. As discussed in Section 3.2, we expect the same behavior for Y following the same arguments presented for Sr. Figure 3.4 shows our values with the error bars compared to values from three different halo samples. Sr and Y should form through the same mechanisms, we expect them to behave similarly. Unlike Sr, the relative abundances of Y show no noticeable trend with metallicity. Another difference compared to Sr is that the scatter between the individual stars seems to be constant over the metallicity range and smaller, covering a range of $\sim$ 1dex.

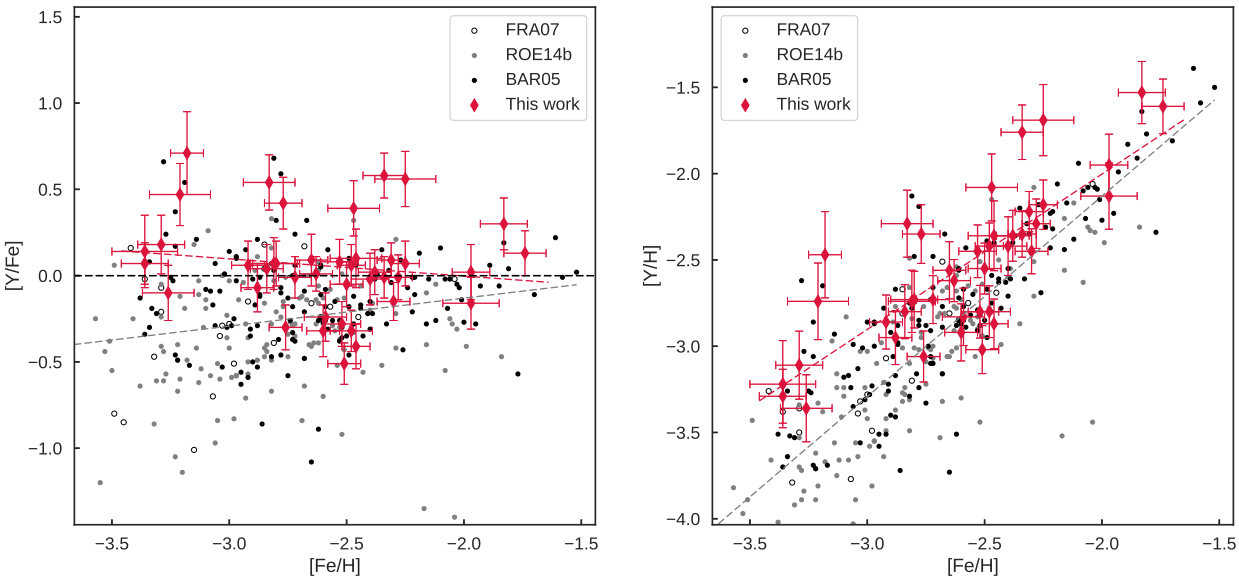

Figure 3.4: The red diamonds show the measured values from this work with uncertainties. The black circles are taken from Barklem et al. (2005), the white circles from François et al. (2007) and the gray circles from Roederer et al. (2014). The dashed line shows the Solar value.

In comparison to the halo samples, our results only agree with the scattered behavior of the halo stars. The main difference is that the halo stars show a decreasing trend with decreasing metallicity similar to what is seen in the Sr plot. This is seen in all three halo samples, on the other hand our sample does not show this kind of behavior. In fact our stars show the opposite behavior, where [Y/Fe] shows a small increase with decreasing metallicity. This increase is within the uncertainties values, more stars with [Fe/H]< -3 are needed to confirm this behavior.

The main result from Figure 3.4 is that as MP halo stars, our sample shows a scattered pattern covering a relatively wide range, although smaller than the scatter shown for Sr. Unlike Sr, we do not see a decreasing trend for [Y/Fe] with metallicity. We discuss the comparison between Y and Sr in more detail in the following chapter.

We have used nine Y absorption lines to measure the abundances, these lines cover a wide range of the spectrum from 3700Å to 5200Å. The atomic data for the lines can be found in Table B.1. In Figure 3.5 we show an example for the fits of the lines. We were able to measure Y for 41 of our stars.

3.4 Ba

In Figure 3.6 we show the results for Ba from 46 stars. The first thing we notice is that the scatter between the Ba abundance for individual stars increases with decreasing

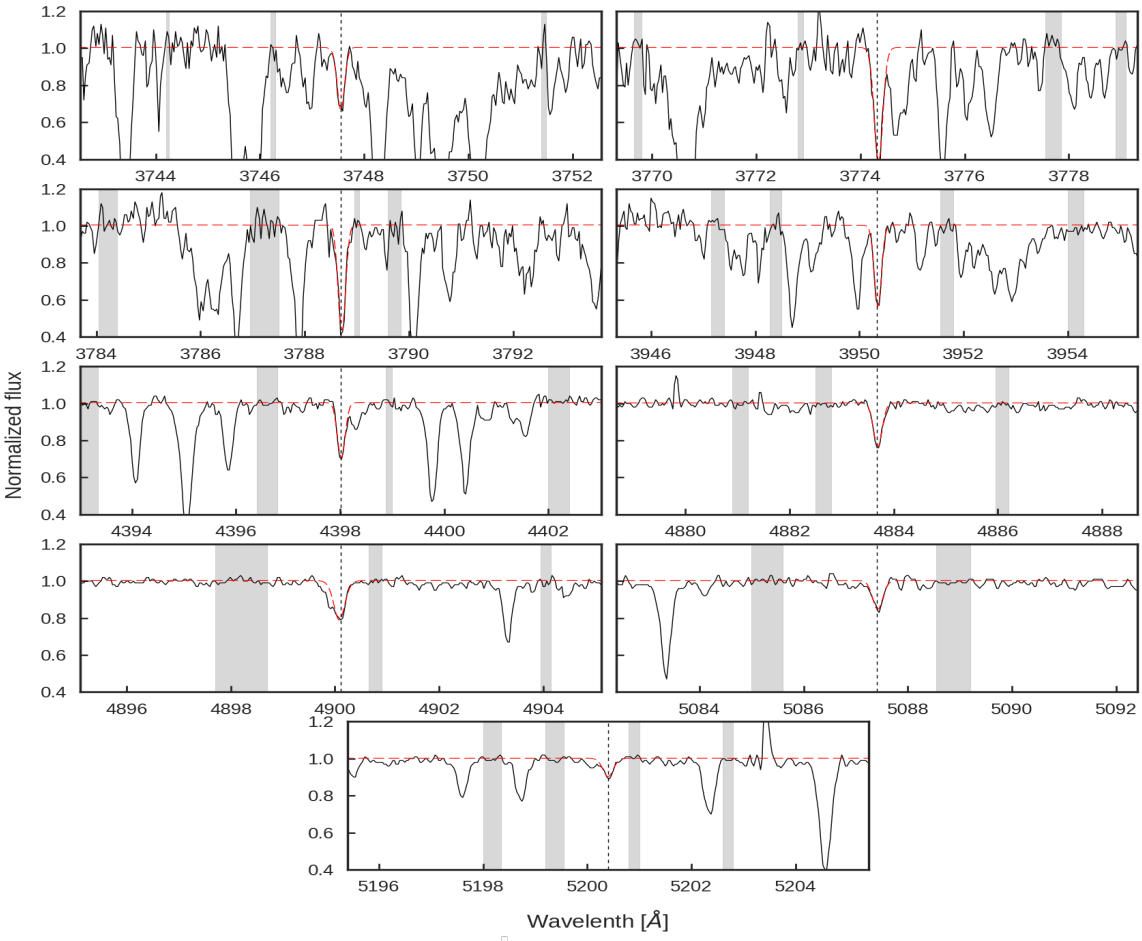

Figure 3.5: The figure shows an example for the fit of the nine Y lines that we use for the abundance measurements, the observed spectrum is shown in black and the fitted spectrum in red. The gray regions mark the continuum masks. This fit is for star SMSS J183647.89-274333.1 with a SNR of 43 and [Y/Fe]= 0.06.

metallicity, similar to Sr. In contrast to Figure 3.2, [Ba/Fe] shows a noticeable trend with [Fe/H], mainly the relative abundance of Ba to Fe decreases with metallicity. This behavior is similar to what is observed in MP halo stars, although our stars show a smaller scatter. The standard deviation about the best fit of our sample is 0.44 compared to 0.55 for the halo sample.

Ba is an s-process dominated element, meaning that in the earliest times we only expect a small abundance that is produced by the r-process. This is what we see in the figure, that the most MP stars have lower relative Ba abundances. Although Sr and Ba are both formed through the s-process, each belongs to a different s-process peak (the first and second respectively). If they are formed through the same mechanism during the earliest times in the Galaxy, both elements would behave similarly. This is understood better by studying the [Sr/Ba] trends, we discuss this in the following chapter.

Similar to our main result from the Sr plot, the Ba abundances for MP bulge and halo

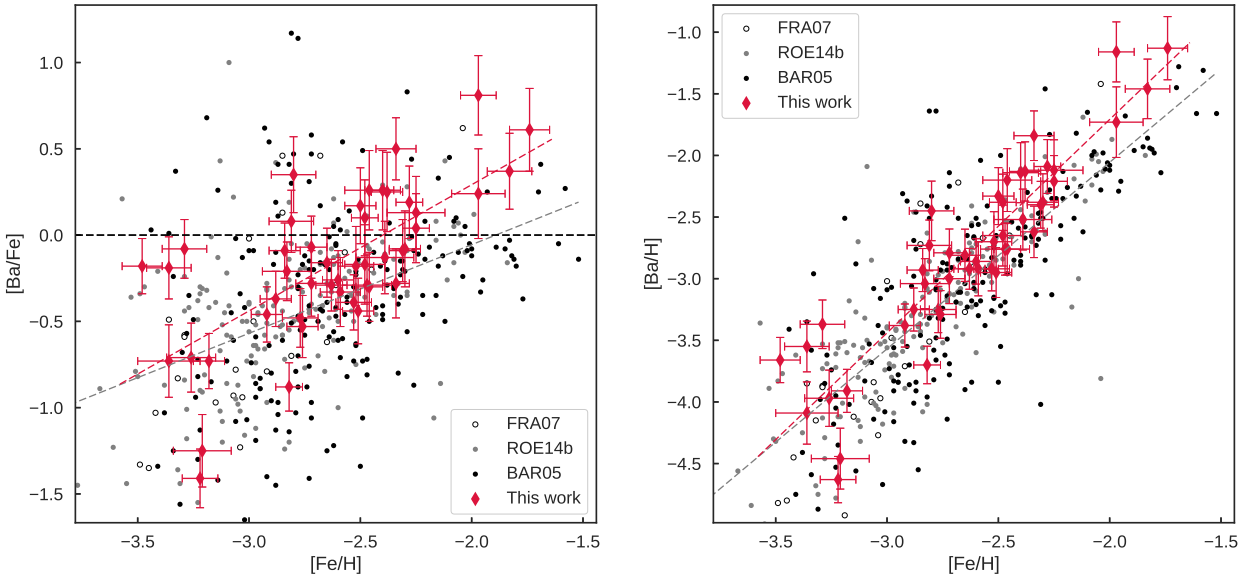

Figure 3.6: Symbols as in Figure 3.2. Our results show a scatter towards lower metallicities as in the halo stars, with a significant trend with decreasing metallicity.

stars show similar properties, although our stars show a smaller scatter than the halo stars.

We show an example for the synthetic spectrum fit for the four Ba lines used for the abundance determination in Figure 3.7. The Ba lines are at 4934Å, 5853Å, 6141Å and 6496Å. The line at 4934Å is the strongest among the lines, in most of the stars this line gives values that are much higher than the other three lines. In such a case when this line does not agree with the others it was not included in the final abundance determination. Isotopic shifts and hfs data are included for Ba as retrieved from VALD. Similar to the fit for the Sr lines, we get the best fit by getting the synthetic spectrum to agree with the observed continuum level within 5Å on both sides of the line.

3.5 Eu

The main goal behind this work is to measure the s-process abundances in this sample of stars from the bulge, to see what we can determine about early stellar nucleosynthesis. This is better understood if we compare the s-process elements to an element that is mostly produced through the r-process such as Eu. Eu transition lines are relatively easy to detect in stellar spectra compared to other r-process elements, making it one of the main r-process elements referenced in the literature.

We show our measured abundances for Eu compared to values for halo stars from the literature in Figure 3.8. Similar to the other n-capture elements, Eu from the halo stars shows a scattered pattern that increases with decreasing [Fe/H] covering a range of $\sim$ 2dex.

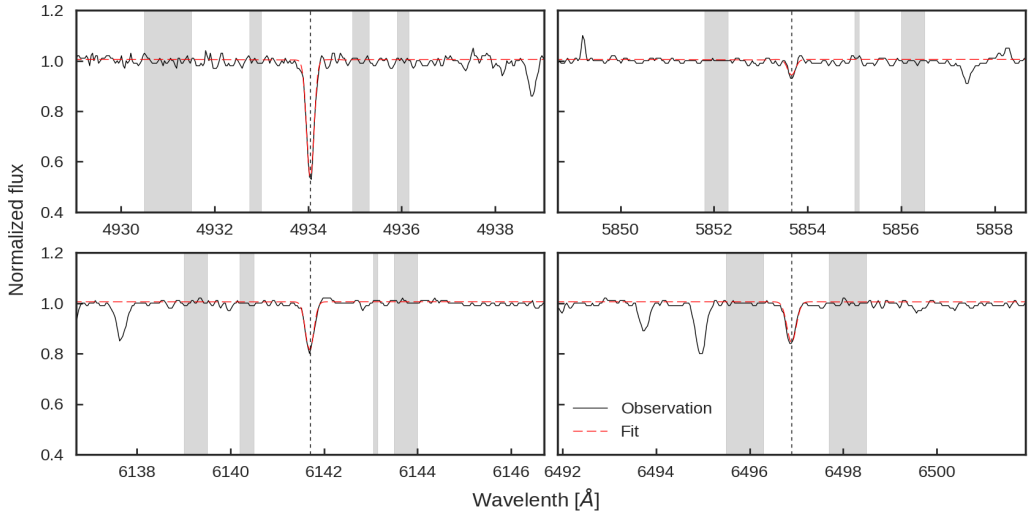

Figure 3.7: The figure shows an example for the fit of the four Ba lines that we use for the abundance measurements, the observed spectrum is shown in black and the fitted spectrum in red. The gray regions mark the continuum masks. This fit is for star SMSS J175021.86-414627.1 with a SNR of 93 and [Ba/Fe]= −0.26.

This behavior is similar to what we see in our sample with a more narrow scatter covering a range of $\sim$ 1dex.

Aside from the scatter our values show a decreasing trend with decreasing metallicity, this behavior is seen in the two halo samples from Barklem et al. (2005); François et al. (2007)). The sample from Roederer et al. (2014) shows a different behavior as [Eu/Fe] slightly increases with decreasing [Fe/H]. This contradiction between the halo samples is mostly due to the wide scattered abundances, hence the trends are not of much use for us. The mean [Eu/Fe] value from our sample is higher than the average from the halo samples, with two stars that are highly enhanced in Eu. The mean of our stars' [Eu/Fe] is 0.69 compared to 0.39 for the halo stars, the value from our sample is 75% higher than that from the halo sample.

In Figure 3.9 we show an example for the fits to the four Eu lines used to measure the abundances. The following four lines are used 3819.65Å, 3907.12Å, 4129.69Å and 4205.04Å. The atomic data for these lines is listed in Table B.1, we include isotopic shifts for the Eu lines, these values are as retrieved from VALD.

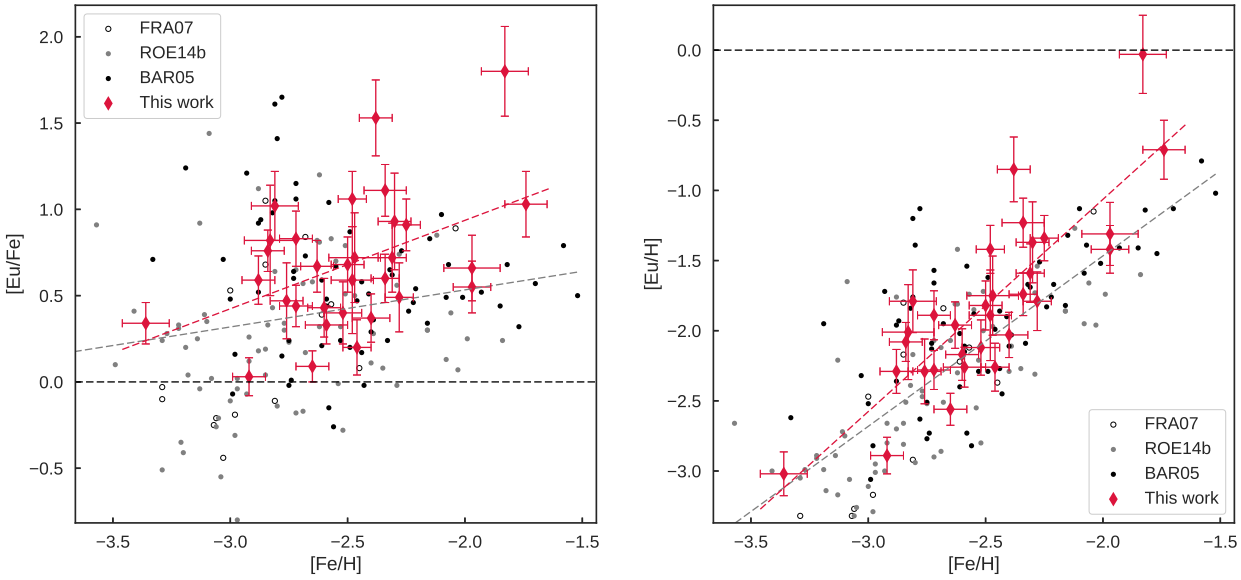

Figure 3.8: Symbols as in Figure 3.2. Overall our sample matches the scattered behavior from the halo samples within the covered metallicity range. One star has an exceptionally high Eu abundance as seen in the [Eu/H] plot.

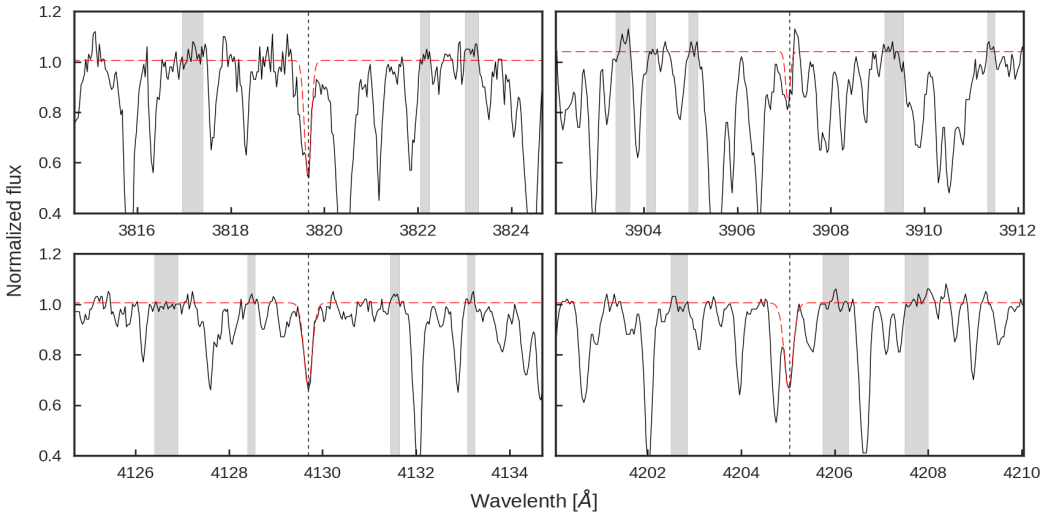

Figure 3.9: The figure shows an example for the fit of the four Eu lines that we use for the abundance measurements, the observed spectrum is shown in black and the fitted spectrum in red. The gray regions mark the continuum masks. This fit is for star SMSS J181946.17-340737.3 with a SNR of 87 and [Eu/Fe]= 0.91.

Chapter 4

Discussion

4.1 Element/Element comparison

To better understand our results, an element to element comparison is the best way of doing so, as such plots carry more information than the commonly used [X/Fe] vs. [Fe/H] plots. We first start by comparing the first s-process peak elements Sr & Y with each other then compare them to the second s-process peak element Ba. We also discuss the relative abundance of Eu to that of Ba, in the literature this comparison defines the classification of an s or r-process enhancement. We discuss these plots with the main question behind this work in mind; were spinstars among the first stars in the Universe?

4.1.1 Light s-process (Y/Sr)

Both Sr and Y are light s-process elements, the comparison between their abundances helps in understanding the process through which they form. In Figure 4.1 we plot our abundances against the literature sample, we also plot the best linear fit to our data and that for the literature data. It can be clearly seen that the best fit to the literature data is flat with a slope of 0.01, while for our measurements there is an increasing trend with decreasing metallicity with a slope of -0.2.

As the area of the plot below [Fe/H]$\leqslant -3$ is sparsely populated with a wide scatter ($\sim$1 dex), we tested the fit for only the stars with metallicities higher than [Fe/H]$= -3$. This test showed that the anticorrelation between [Y/Sr] and [Fe/H] for our stars is still present with a slope of -0.3 in this case, this behavior is unexpected. To confirm if this trend is real for our stars, we need more stars at the lowest metallicities to populate the area of the plot below [Fe/H]$\leqslant -3$.

If we focus now on the [Y/Sr] vs. [Sr/H] plot in Figure 4.1, the anticorrelation between both quantities is much stronger in our sample (best fit slope=-0.3) than in the halo samples (best fit slope=-0.1). The stars from FRA07 show a similar behavior to our results, extending to lower [Sr/H] with values most of which are upper limits. François et al. (2007) do not comment on what may cause this behavior due to the high number of upper limits at low [Sr/H]. As our stars do not go as low in [Sr/H], this behavior needs

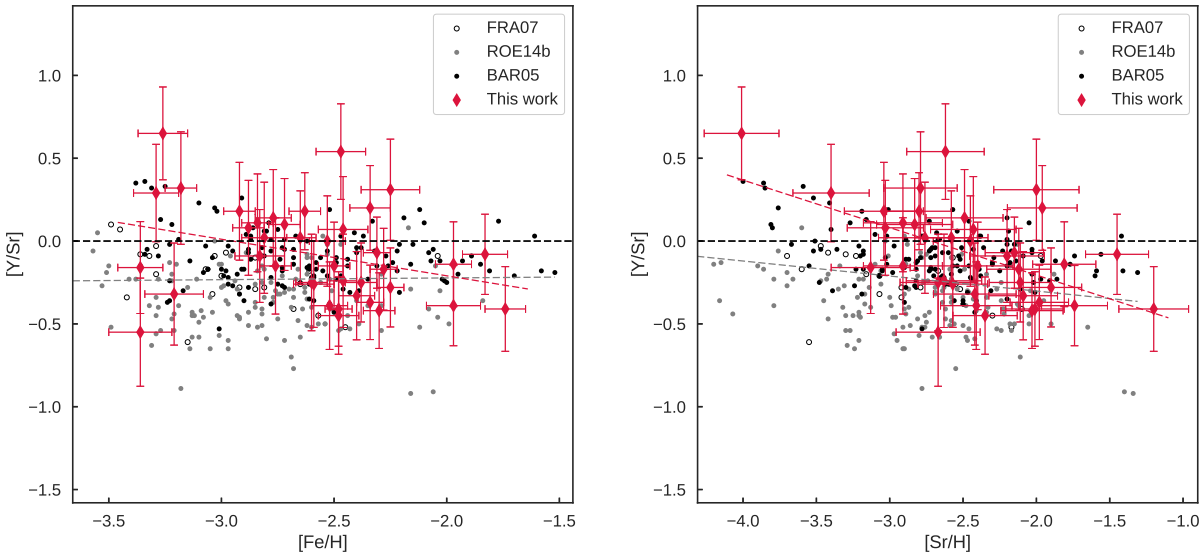

Figure 4.1: We show the relative abundance of Y to Sr for our stars and the literature vs. both [Fe/H] (left) and [Sr/H] (right). The red dashed line is the best linear fit to our data, the black dashed line represents the Solar ratio and the gray dashed line is the best linear fit to the literature. Our stars show an anticorrelation with metallicity unlike the literature data.

further investigation as it might indicate different production ratios for both Sr and Y from either this early light n-capture element process or the r-process.

4.1.2 Light/heavy s-process

The comparison between light to heavy s-process elements is of high interest to astronomers. This is due to evidence of the production of the light elements (e.g. Sr, Y and Zr) without significant production of the heavy elements (e.g. Ba and La) at the lowest metallicities in the halo. In Figure 4.2 we plot [Sr/Ba] and [Y/Ba] vs. [Fe/H]. Our stars show a similar behavior to the halo samples for both [Sr/Ba] and [Y/Ba]. In both plots we can see a scatter that increases with decreasing metallicity and an inverse relation between [Sr,Y/Ba] and [Fe/H].

First we discuss the [Sr/Ba] plot, where our stars behave similarly to the halo samples. One feature that stands out from first inspection of the plot are the three stars with high [Sr/Ba], these three stars are the same three stars in the top left corner of the [Y/Ba] plot. If these three stars are excluded from the best fit, the trend with metallicity flattens out. We discuss the star with highest [Sr/Ba] later in Section 4.1.4. To confirm whether ther really is an anticorrelation between [Sr/Ba] and [Fe/H] in the bulge, more stars with [Fe/H]< -3 are needed.

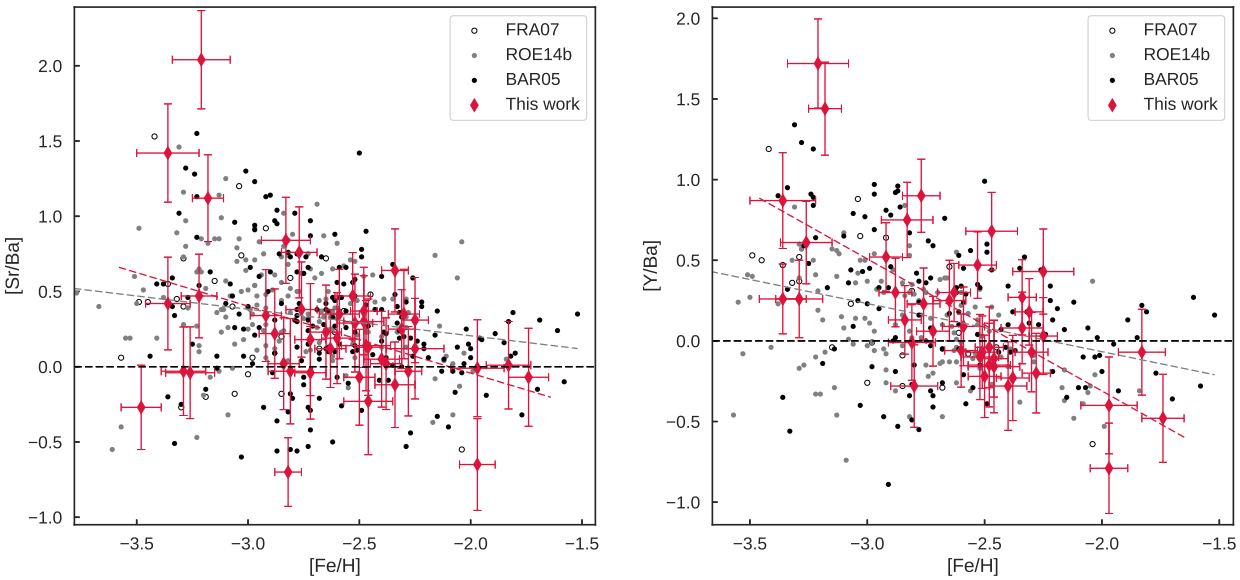

Figure 4.2: The left plot shows the relation between [Sr/Ba] and [Fe/H] for our stars against the literature, while the right plot is for [Y/Ba] vs. [Fe/H]. We plot the best linear fit to our data (red dashed line) and the best linear fit to the literature (gray dashed line). The black dashed line shows the Solar value. Both [Sr/Ba] and [Y/Ba] show an increasing scatter and increasing trend with decreasing metallicity. This anticorrelation is stronger for Y than Sr.

In the [Y/Ba] plot in Figure 4.2, there are two stars that stand out from our sample with high [Y/Ba] values. These two stars have high [Sr/Ba] values as well ([Sr/Ba]$>$ 1). If these two peculiar stars are not included in the best fit for Y, however, the trend is not affected. This supports the possibility that the [Sr/Ba] trend is real and not only due to the three stars with high [Sr/Ba]. These two light s-process enhanced stars do not have Eu measurements. In the star with highest [Sr,Y/Ba] the Eu lines are too weak to measure, in the other star the SNR is too low in the Eu lines wavelength region.

Due to the [Y/Ba] trend not being affected by the two stars with high [Y/Ba], we believe that the [Sr/Ba] and [Fe/H] anticorrelation is real as well. Yet more data points at the lowest metallicity are needed to further confirm this behavior for our stars.

The light-to-heavy s-process elements comparison raises many questions. The anticorrelation between Sr(Y) and Ba points towards two different production sites/mechanisms for the light and heavy s-process elements at the earliest times before the main s-process in AGB stars kicks in. More information on the properties of this unknown process can be found be removing the scaled Solar system r-process yields from each star's abundances. In François et al. (2007) this is done by assuming all the Ba in each star is produced by the r-process, this helps to untangle the production of the light s-process elements from Ba. This assumption is mainly based on the idea that the r-process is the main source for heavy elements in these MP stars.

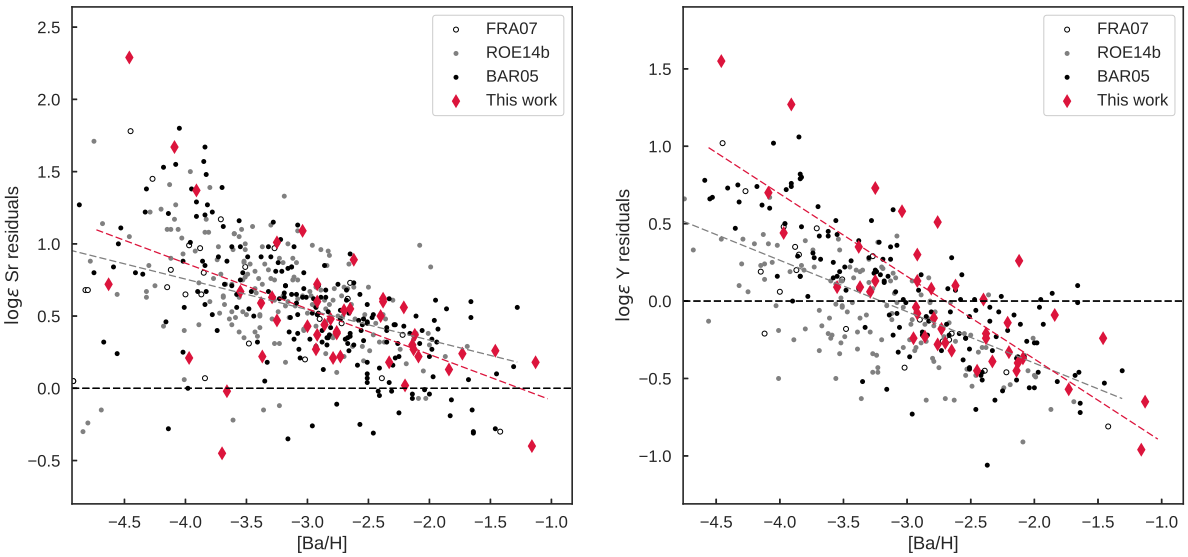

Figure 4.3: In this plot we show the residuals for both Sr and Y by subtracting the r-process scaled value for each star. The best linear fit to our data (red dashed line), best fit to literature (gray dashed line) and the solar value (black dashed line). There is a strong anticorrelation between both Sr and Y and Ba. These plots are the main reason for suggesting the need for a separate light s-process production site at the lowest metallicities. See the text for more details.

We follow the same assumptions as in François et al. (2007) to calculate the residuals shown in Figure 4.3. The r-process is scaled such that all the Ba in a star is formed though the r-process, by setting $\log \epsilon Ba_{\odot r-process} = \log \epsilon Ba_* = 0$. The scaled $\log \epsilon X_* = \log \epsilon X_{*orig} - \log \epsilon Ba_*$, the same step is followed to scale the Solar system r-process yields for the other elements as well.

The residuals shown in Figure 4.3 are then the result from $\log \epsilon X_* - \log \epsilon X_{\odot r-scaled}$. If Sr and Y are formed mainly through the r-process in these stars the residual values should scatter around [X/Fe]=0, this clearly is not the case as seen from the figure. This means that the extra residuals for Sr and Y must have a different origin other than the main r-process. Although the definite origin of the r-process is yet to be confirmed, the inferred yields from the Solar abundances match well with the heavy r-process elements.

To calculate the Sr and Y residuals for each star we use the Solar system r-process element fraction as from Sneden et al. (2008). After removing the r-process' contribution to each star's heavy elements abundances, the anticorrelation between the light and heavy s-process elements is still strongly present. In François et al. (2007), they mention that this unknown light n-capture production site is responsible for $90-95\%$ of the total abundance of these light elements at the lowest [Ba/H]([Fe/H]) values.

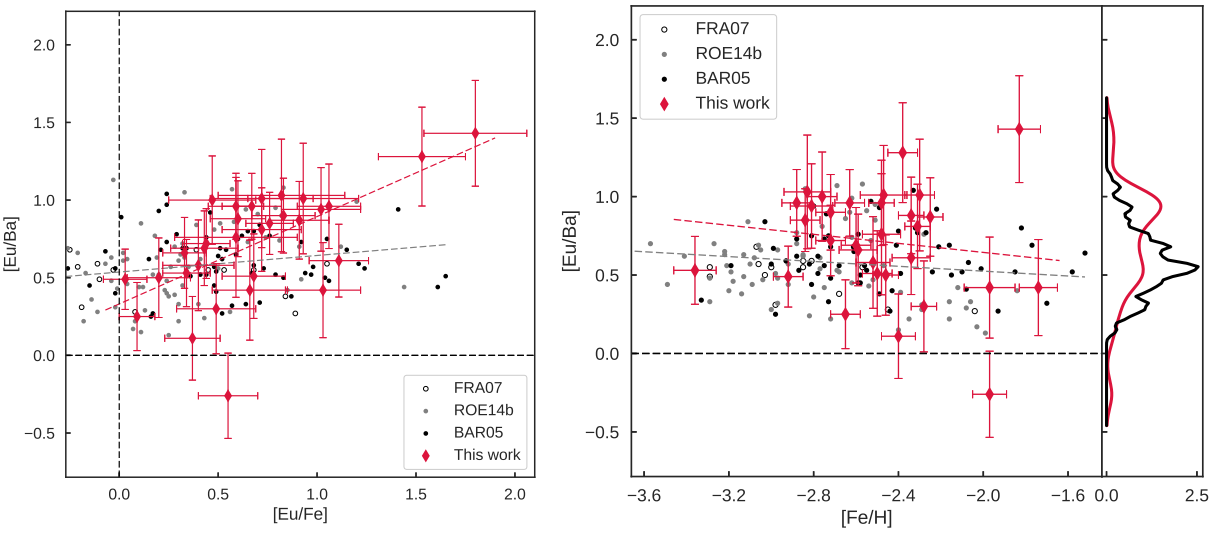

Figure 4.4: To the left we show our values for [Eu/Ba] vs. [Eu/Fe] and to the right [Eu/Ba] vs. metallicity (same legend). Attached to the right plot are two kernel density estimates, one in black for the literature data and the other in red representing our data. See the text for detailed discussion

4.1.3 [Eu/Ba]

In Figure 4.4 we plot our [Eu/Ba] abundances vs. [Eu/Fe] to the left and as a function of metallicity to the right, on the right side of the plot we add a kernel density estimation (kde) to better visualize the data. According to Beers and Christlieb (2005), MP stars can be categorized by specific element signatures, such as being r or s-enhanced. Stars that are r-enhanced are divided into two categories r-I and r-II. MP r-I enhanced stars are those with 0.3 <[Eu/Fe]< 1.0 and [Eu/Ba]> 0, r-II enhanced stars are those with [Eu/Fe]> 1.0 and [Eu/Ba]> 0.

As we can see from the left plot in Figure 4.4, only 4 out of 31 of our stars fall outside of these limits. The majority of our stars (21 stars) are r-I enhanced and 6 stars are r-II enhanced. In order to better understand this r-enhancement, we now focus on the right plot in Figure 4.4. This plot shows [Eu/Ba] vs. [Fe/H] with two kde's plotted to the right of the plot. The black kde represents the literature data points and the red kde represents our data. By inspecting the scatter plot, aside from the star with the highest [Eu/Ba] and the star with the lowest [Eu/Ba] our stars show a similar scatter to the halo literature. However, the majority of our stars (50%) are moderately r-enhanced with [Eu/Ba]> 0.6, with six stars having [Eu/Ba]> 1.

The kde plot in the right plot of Figure 4.4 is one of our most interesting and unexpected results. The kde for our data shows two peaks in [Eu/Ba] unlike the literature data's kde that has only one peak at [Eu/Ba]=0.54. The first peak from our data at [Eu/Ba]=0.53 agrees well with the peak from the literature data, although having a much smaller am-

plitude. The second peak that is seen for our data is at [Eu/Ba]=0.94, the literature data shows no significant peak at this high [Eu/Ba] value. This result could help us untangle the puzzle of the r-process production site/s.

This moderate r-enhancement in the majority of our stars and significant peak at [Eu/Ba]=0.94 in the kde point towards strong r-process production sites that produce high yields. Neutron star (NS) mergers and magnetorotationally driven SNe (MRDS) are two sites with such a property (Wehmeyer et al. 2015). However, there seems to be some conflict in the literature on which of these sites is the dominant r-process source in the early Universe. Argast et al. (2004) show that in the early Universe CCSNe are more likely to be the main source for the r-process compared to NS mergers, mainly due to the low rate of NS mergers. According to them the contribution from NS mergers is expected to be more significant at higher metallicities due to their long lifetimes. On the other hand, Ishimaru et al. (2015) show that by employing a hierarchical galaxy formation scenario (the galaxy forming through the merger of sub-halo structures), NS mergers could be the dominant r-process production site throughout the Galaxy's history.

Ji et al. (2016) study the n-capture abundances in an ultra faint dwarf galaxy (these dwarf galaxies are believed to be the building components of galaxies), they predict that the high Eu and Ba abundances they find could be due to a NS merger event. This result supports the conclusion from Ishimaru et al. (2015), that NS mergers in sub-halo structures such as dwarf galaxies are an efficient r-process production site. However, similar to Ji et al. (2016), our results only can not distinguish between NS mergers or MRDS. The r-process yields from MRDS and NS mergers are similar. More studies on the yields of each site, particularly work on their differences is needed to better understand the r-process production site in the early Universe.

4.1.4 Peculiar stars

We find a few stars that show different abundance patterns than the majority of the stars, here we discuss these stars.

The star SMSS J175636.59-403545.9 ([Fe/H]= −3.21) shows exceptionally high [Sr/Ba]= 2.04, only a few stars exist in the literature with such a value. This star has a high [Y/Ba]= 1.72 and is slightly carbon enhanced with [C/Fe]= 0.65(from Howes et al. 2015). According to Cescutti et al. (2013), their models predict that stars with high [Sr/Ba] should show the pollution of the s-process in spinstars. This star is a good candidate to test this prediction, by measuring the odd-to-even isotopes ratio of Ba. This test is relatively challenging as even with the highest resolution and SNR spectra the isotopic abundances may still suffer from large uncertainties. This leaves us with a potential signature that is challenging to confirm.

We find two r-enhanced stars SMSS J18312.87-341018.4 ([Fe/H]= −1.83) and J18205146-3407333 ([Fe/H]= −2.38) that have the highest [Eu/Fe] of 1.8 and 1.53 respectively. Both stars have the highest [Eu/Ba] as well and show no carbon enhancement. These two stars with metallicities around [Fe/H]= −2 are good candidates for the signatures of r-process production in NS merger.

The star SMSS J182637.10-342924.2 with [Fe/H]= −1.97 has the highest Ba abundance. It also shows the lowest [Y/Ba]= −0.79, with low [Sr/Ba]= −0.65 and low [Eu/Ba]= −0.26. This star is slightly carbon enhanced with [C/Fe]= 0.68, the low [Sr/Ba] and high [C/Fe] make this star a member of the CEMP-s (carbon/s- enhanced MP) class, in the literature the majority of these stars are in a binary system (Sneden et al. 2008). Another peculiar star is SMSS J181406.68-313106.1 ([Fe/H]= −2.82). This star is poor in both Sr and Ba with [Sr/Fe]= −1.58 and [Ba/Fe]= −0.88, Y and Eu are not detectable in this star, so further studies would be needed to understand the low abundances, especially the upper limits for Y and Eu would be of great importance.

4.2 Comparison with spinstars models

The main question behind this work is whether we see any signatures of spinstars yields in our sample or not. To answer this we plot our abundances for each element against yields from two GCE models one for the halo (for details see Cescutti and Chiappini 2014) and another representing an old bulge population (Cescutti priv. comm.). We then compare the element to element ratios with the spinstars models as well.

These GCE models predict the enrichment history of the ISM in one region of the Galaxy. This is produced by simulating the predicted yields from magnetorotationally driven SNe (MRDS) as the r-process production site and the yields from spinstars, in addition to a predicted initial mass function for the early times in the Galaxy. The models can then calculate the amount of elements produced at each time step in the simulation. The yields from each generation enriches the ISM, from which a new generation of stars is formed. This process goes on until the ISM reaches a metallicity around Solar.

These models simulate the Galaxy's chemical evolution in two different regions, one modeling the halo and the other for the bulge. For the r-process the model includes the yields from MRDS, assuming 10% of all the stars in the mass range 10-80$M_{\odot}$ end their life as MRDS producing an r-process with varying yields. Along with the r-process they include the s-process yields produced by spinstar models. For the bulge model, the metallicity range stops at [Fe/H]= −3, this is due to the bulge being denser than the halo and the model having a higher SFR (supernovae taking place in a denser region would enrich it in metals faster).

The point of these comparison plots is to see if by including the yields from spinstars these models can explain our results. As shown in Section 4.1.2, our stars show the same behavior as halo stars with an increasing trend with decreasing metallicity for the light s-process (ls) elements relative to Ba. This behavior is one of the main arguments for the need of an s-process production site at the earliest times, as it would enhance the ISM with ls elements.

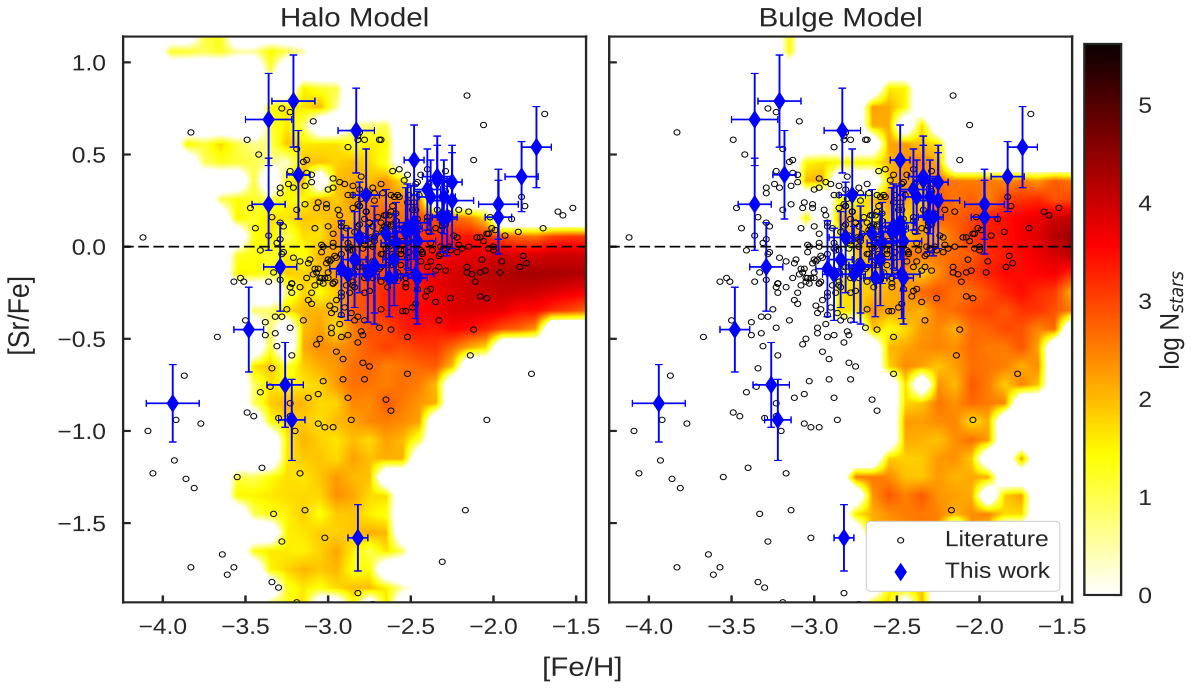

Figure 4.5: We plot our results for Sr in comparison with the models from Cescutti and Chiappini (2014). Our stars are represented by the blue diamonds, the literature data by the black circles and the model as a color map. The black dashed line shows the Solar value. The left plot shows the halo model and the right plot with the bulge model. The halo models seems to match our data better than the bulge model, except for the stars with the highest metallicity. These higher metallicity stars are better explained by the bulge model.

4.2.1 Sr, Y

In Figure 4.5 we plot our Sr abundances compared to the yields from both the halo and bulge models. At first sight, the halo model seems to match our results better than the bulge model, even predicting the star with lowest Sr abundance. If we focus on stars with [Fe/H]> -3 (the metallicity region mapped by the bulge model), the bulge model does a fairly good job in predicting the majority of our stars, especially the stars with the highest metallicity. These high metallicity stars are not predicted by the halo model.

The same is seen for Y in Figure 4.6. Within the metallicity region mapped by the bulge model, the higher metallicity stars are matched better than the lower ones. The halo model agrees well with our stars, except for the stars with metallicities around [Fe/H]$= -2$ that fall out of the model predictions.

In the plots for Y the halo sample shows stars around [Fe/H]$= -3$ with low [Y/Fe] abundances, these are also predicted by the halo model. Our sample has no stars in this part of the plot, this could be due to the lack of stars in this metallicity region or that our sample is truly more Y enhanced compared to the halo sample.

One common feature in both plots for Sr and Y compared to the halo model, is that

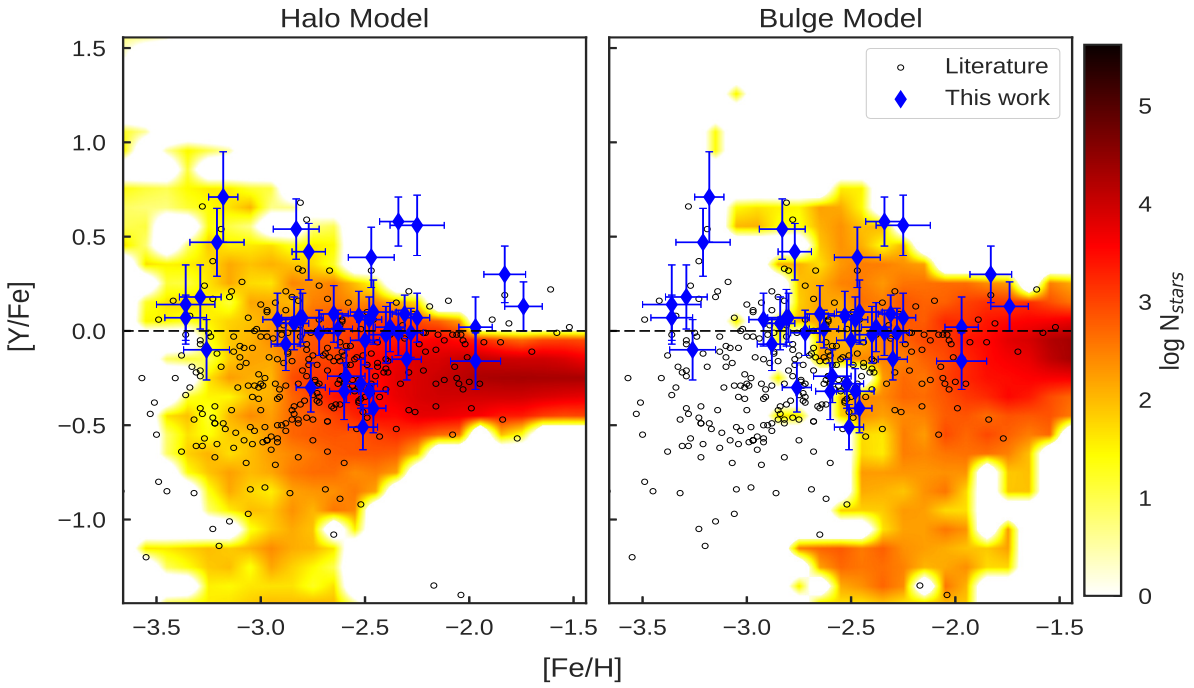

Figure 4.6: Symbols as in Figure 4.5. The stars in the upper right corner are better matched by the bulge model, yet the majority of our stars are best predicted by the halo model.

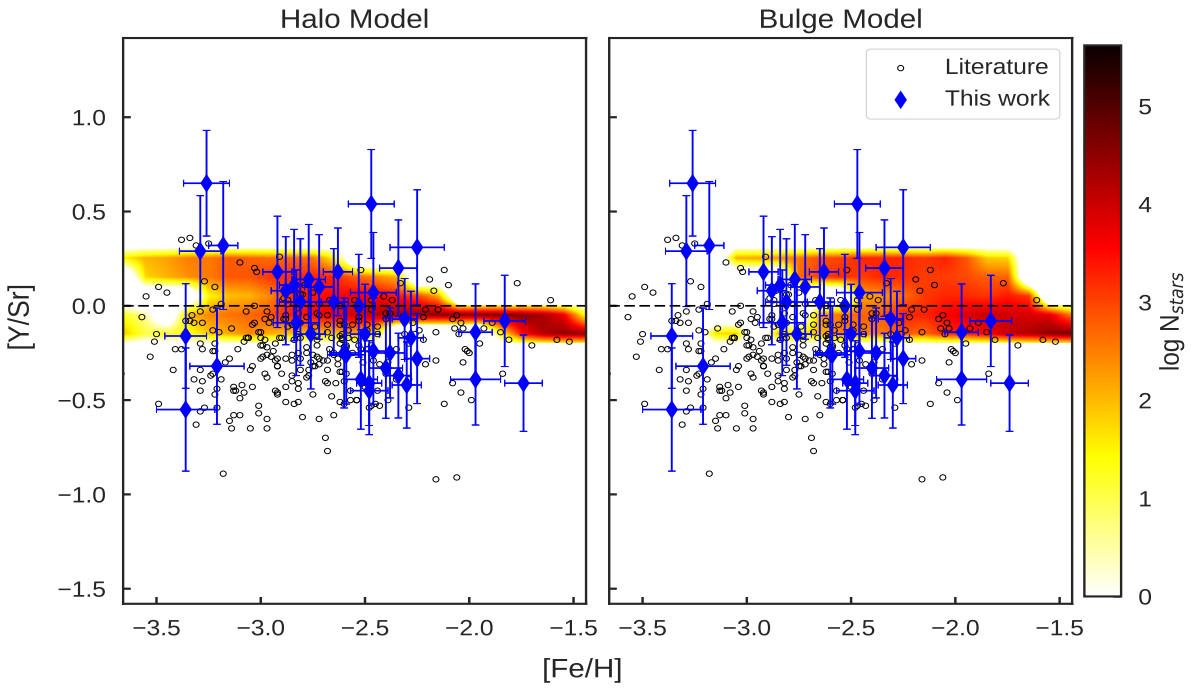

Figure 4.7: Symbols as in Figure 4.5. Within the error bars the halo model matches the majority of our stars above [Y/Sr]~ -0.3, the bulge model is a bad match to our stars. The scatter from our results is wider compared to the model predictions.

the halo model fails to predict the stars with the highest metallicity ([Fe/H]> -2). The bulge model does not map the lowest metallicity regions and seems too focused on higher metallicities. Different models, perhaps using our results as constraints, may aid in getting more realistic predictions. The halo model is a better match to our results for Sr and Y, yet the bulge model is not far off.

In Figure 4.7 we compare our [Y/Sr] measurements with the models. The bulge model shows a poor match to our results, the halo model is little better. The halo model does not predict anything in the lower part of the plot below [Y/Sr]~ -0.3, the stars that are enhanced in Sr relative to Y. The scatter of our results is much bigger than that predicted by the models. Both models predict the [Y/Sr] from the r-process to be constant, the scatter seen in the models is from the spinstars s-process. The yields from the r-process for Y and Sr is not constant, which is what we can see here as a wide scatter in both our stars and the halo sample.

The models need to incorporate that the r-process Y to Sr ratio is not constant, this may help in predicting the stars in the lower half of Figure 4.7 or the wide scatter. The models assume an inhomogeneously mixed ISM, which explains the small spread in the models predictions. Maybe this wide scatter in our results is a result of a different s-process production site with a wider Y to Sr scatter. Nevertheless, The bulge model needs more work than the halo model to better match our results.

4.2.2 Ba, Eu

In Figure 4.8 we plot our Ba results against the models. The bulge model fails to predict the majority of our stars. The halo model is a better match to the stars within the metallicity range $-3 <$ [Fe/H] $\lessapprox -2.2$, although similar to Sr and Y, it does not predict anything close to our highest metallicity stars. Our results show a narrow scatter with a decreasing trend with metallicity, whereas the models predict a much wider scatter. Both models fail to predict our stars with the lowest metallicities.

Similar to Ba, the bulge model fails completely in mapping our results for Eu. The halo model is better in mapping our stars, except for the highest metallicity ones. The models include MRDS as the main r-process source at the early times, this good match between the halo model and our stars is an important result as it supports the idea of MRDS being a source for the r-process at the early times. The halo model fails to predict 3 stars towards the higher metallicities, this mismatch may point that the models need to include another r-process production site that is more efficient and stronger at these higher metallicities.

In Figure 4.10 we plot our [Eu/Ba] abundances compared to the predictions from both the halo and bulge model. Both models show a poor fit to the data, particularly the bulge model. The halo model only predicts values in a narrow band around [Eu/Ba]~ 0.6. It fails to match the stars with the highest [Eu/Ba], as well as the lowest [Eu/Ba]. The models assumes a constant [Eu/Ba] from the r-process, this prevents it from predicting the r-enhanced stars.

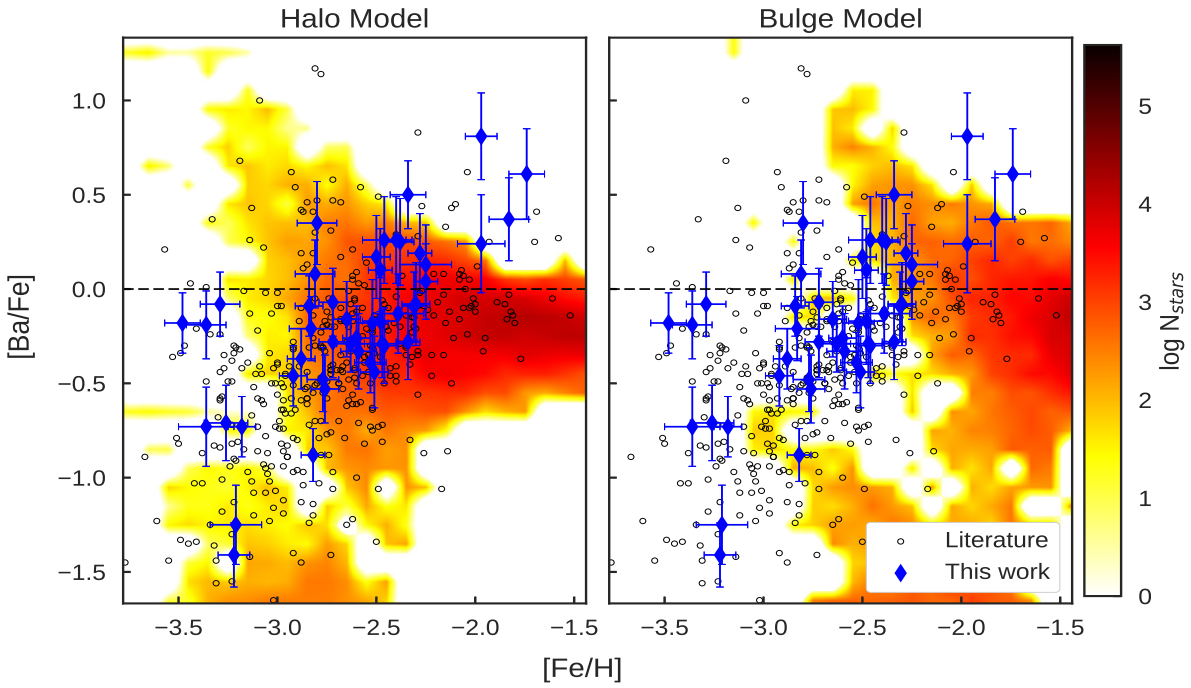

Figure 4.8: Symbols as in Figure 4.5. The halo model is a better match to our results than the bulge model, except for the stars with highest metallicity.

4.2.3 [Sr/Ba], [Y/Ba]

Do we need to include the yields from spinstars to explain our results? We try to answer this question in this section. The anticorrelation between [Sr/Ba]([Y/Ba]) and [Fe/H] is the best method to check for the need of spinstars, as in the literature these plots are used to justify the need for an early light s-process production that is different than the main r-process (Travaglio et al. 2004)

In Figure 4.11 we plot the [Sr/Ba] abundances against the models predictions. As one would expect following from the individual elements comparison to the models, the halo model matches our data better than the bulge model. Both models fail to predict the stars that are enhanced in Ba relative to Sr (the lowest [Sr/Ba] stars), although as mentioned in Section 4.1.4, these maybe due to binary mass transfer. The two stars with the highest [Sr/Ba] are not predicted by the halo model.

The same behavior is seen for [Y/Ba] as shown in Figure 4.12. The halo model is a better fit to our data, yet it fails to match the stars with the highest and lowest [Y/Ba] values. The bulge model in both [Sr/Ba] and [Y/Ba] looks as if it is shifted towards higher metallicities, providing a very poor fit to the stars. According to Cescutti et al. (2013) the stars with highest [Sr/Ba] are more likely to show the signature of the s-process in spinstars. This could be checked by comparing the odd/even Ba isotopes, which is quite challenging to obtain. Hence the star with the highest [Sr/Ba] and [Y/Ba] is the best candidate to carry the signatures of spinstars, nevertheless, the models fail to predict this star. This suggests that this star might result from a different evolution history. For example,

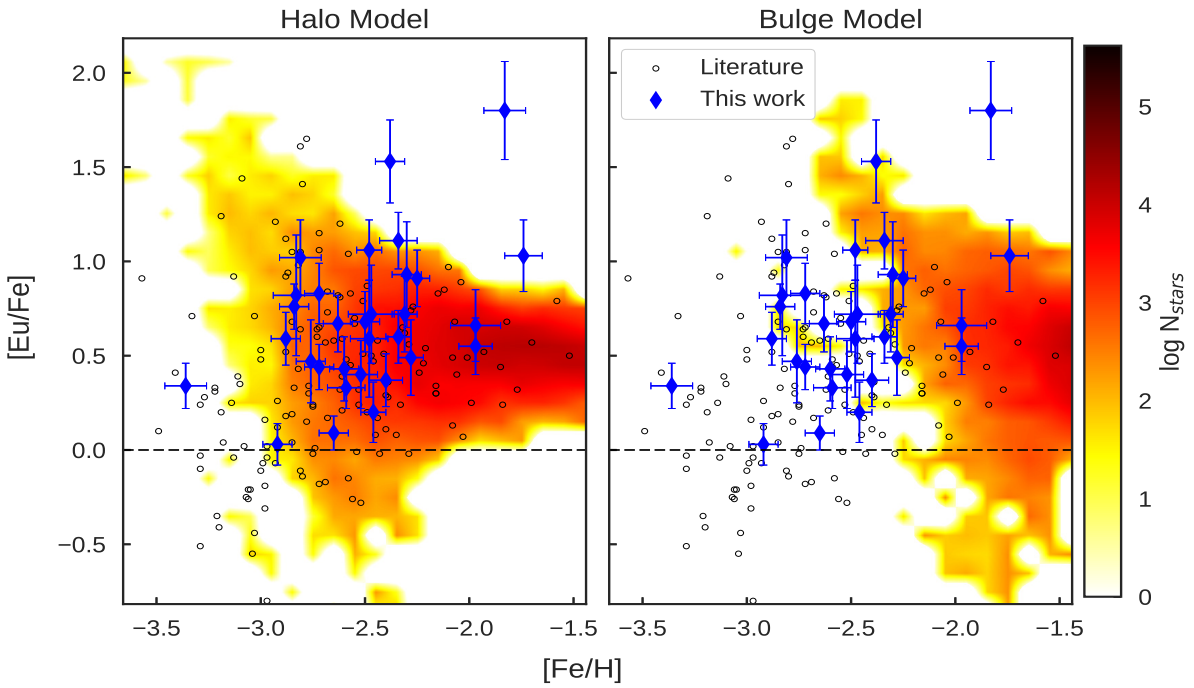

Figure 4.9: Symbols as in Figure 4.5. For the majority of our stars the halo model is a better fit except for the three stars in the upper right corner that fall far out the model predictions. The bulge model fails to predict the majority of our stars.

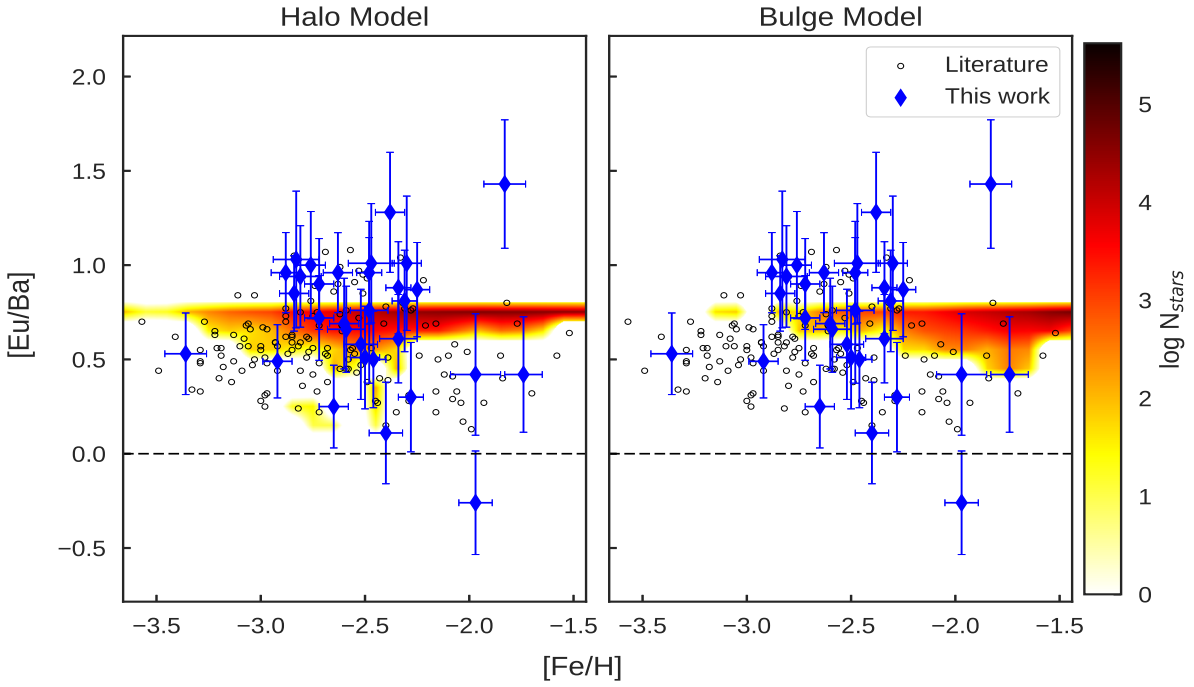

Figure 4.10: Symbols as in Figure 4.5. The predictions from both the halo and bulge models are poor. The bulge model is far off from the data. The halo model fails to predict anything higher than [Eu/Ba]$\sim$0.8 or lower than [Eu/Ba]$\sim$0.5.

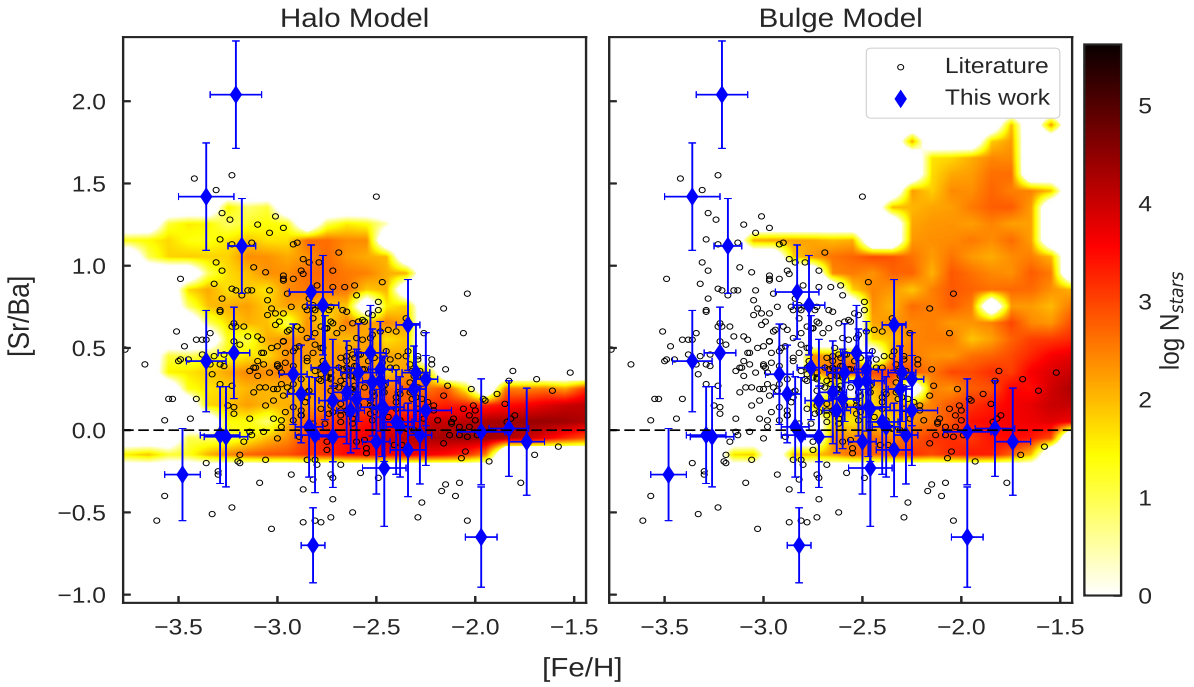

Figure 4.11: Symbols as in Figure 4.5. The halo model is a better match to our stars than the bulge model. It fails to predict the stars with highest and those with lowest [Sr/Ba].

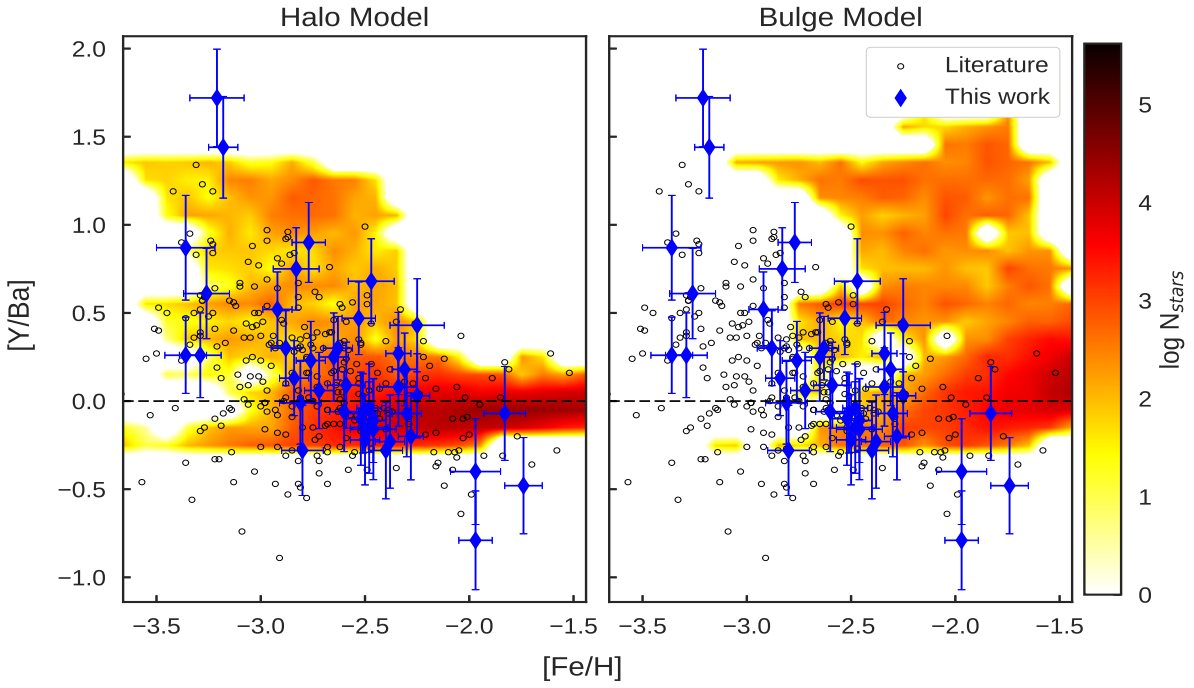

Figure 4.12: Symbols as in Figure 4.5. The halo model is a better match to our stars than the bulge model. It fails to predict the stars with the highest and those with the lowest [Y/Ba].

this star is slightly carbon enhanced, it could be in a binary system causing these high Sr and Y abundances.

In General, from first inspection it seems as if both the halo and bulge have undergone similar n-capture chemical enrichment processes, we came to this conclusion based on two main reasons: 1)The GCE halo model is in good agreement with our stars for Sr, Y and Eu in the [X/Fe] plots, not so much for Ba; 2)Our stars behave similarly to the halo stars, for all of the elements both samples are not easily separable from each other. However, the element-to-element comparison plots show significant differences between our stars and the halo stars; 1-The wide scatter in our [Y/Sr] values compared to the halo, 2-The two peaks in our [Eu/Ba] kde compared to only one peak for the halo samples. The GCE model for the bulge needs improvements, as it seems that to explain our results a mixture between the GCE halo and bulge models is needed.

These points bring us closer to understanding the different components of our Galaxy. Using the results from this work and Howes et al. (2016) to constrain the bulge models would be of great importance to better understand the chemical evolution of the bulge. Hence better models for the bulge are needed to address whether spinstars were amongst the first stars or not, as it seems that including them with the r-process helps in explaining some of the features in MP halo stars specially the wide star-to-star scatter seen at the lowest metallicities.

Chapter 5

Conclusions

Recent galaxy formation simulations show that not all MP stars date back to the earliest times in the history of a galaxy, in other words they form over a wide range of redshifts (e.g. Tumlinson 2010; Starkenburg et al. 2017). These simulations when applied to the Milky Way predict that the oldest MP stars are those on tightly bound orbits in the inner regions of the Galaxy, the bulge. Finding these MP stars in the bulge is a troublesome task as the optical lines of sight towards the bulge are mostly blocked by dust and the bulge is on average metal-rich. The hunt for MP stars in the bulge is like a search for a needle in a haystack, observers need to employ special techniques to find them (Howes et al. 2014). In this thesis we determined the abundances of four of the most commonly measured neutron capture elements in the literature, Sr, Y, Ba and Eu in 48 MP stars from the bulge (for details on observations see Howes et al. 2016). This is the first time n-capture elements have been studied in MP bulge stars.

We compared 10 of our stars to the corresponding measurements from Howes et al. (2016). This comparison showed that by following the same abundance determination technique and using similar atomic data for Ba, the measurements from both studies agree very well. Both studies use different measuring techniques for Sr, Y and Eu, this results in our measurements being on average 0.2 dex higher than Howes et al. (2016)'s measurements for these elements. We have measured the uncertainties in our abundances due to the uncertainty in each of the stellar parameters separately, then added them in quadrature.

Our results show that both our stars and the halo sample mostly have similar s-process properties with some minor differences regarding Y. This to some degree points towards the idea that both regions, the halo and bulge, have undergone similar chemical enrichment histories regarding these heavy elements. In other words, we can say that to some degree the n-capture properties seen for MP stars seem to be universal throughout the Galaxy. One main difference is that our stars are on average more r-enhanced than the halo stars with $\sim$ 50% of our stars having [Eu/Fe]$\geqslant$ 0.6. This favors strong r-process production sites. Our stars show a slightly lower scatter for Ba than the halo sample. We find a slight anticorrelation between [Y/Fe] and [Fe/H] unlike the halo stars, however there are only 6 stars below [Fe/H]=-3, more stars with Y abundances in this region are need to confirm

this behavior.

The [Eu/Ba] abundances for our stars show an interesting result, when using a kernel density estimation to better visualize the data we find two significant peaks in [Eu/Ba] compared to one peak in the halo sample. The first peak at [Eu/Ba]=0.53 agrees very well with the halo stars' peak, the second peak from our data at [Eu/Ba]=0.94 (with a higher amplitude than the first peak) does not show up in the halo stars. From this and our stars being moderately Eu rich, high r-process production sites such as neutron star (NS) mergers and magnetorotationally driven SNe (MRDS) are more likely to be the source for the r-process in our stars (Wehmeyer et al. 2015). However, using our results only we can not distinguish which of these two is the dominant source in the early Universe, a better understanding of their yields is needed to further investigate this.

We find one star (SMSS J175636.59-403545.9) with exceptionally high [Sr/Ba]= 2.04 and [Y/Ba]= 1.72 that is slightly carbon enhanced with [C/Fe]= 0.65, only a handful of stars exist in the literature with similar values. This star could be in a binary system, which may explain the high carbon and s-process abundances. Another star (SMSS J182637.10-342924.2) shows a slight Ba enrichment compared to Eu ([Eu/Ba]=−0.26) and a strong Ba enhancement compared to Sr ([Sr/Ba]= −0.65) and Y ([Y/Ba]=−0.79) with a slight carbon enhancement ([C/Fe]=0.68), this abundance pattern makes this likely to be a CEMP-s star, which in the literature are mostly associated with being in a binary system. The star SMSS J181406.68-313106.1 is poor in both Sr and Ba with [Sr/Fe]= −1.58 and [Ba/Fe]=−0.88, Y and Eu are not detectable in this star, further studies of this star are needed to understand these very low abundances.

We find an anticorrelation between [Y/Sr] and [Sr/H], this could be due to both elements not being produced with a constant ratio through the main r-process (G. Cescutti priv. comm.). This behavior is reported for the sample of stars from François et al. (2007), however most of the stars in their sample covering the lower [Sr/H] region are upper limits. More stars at the lowest metallicities (low [Sr/H]) are needed to further investigate this interesting behavior.

Abundances for neutron capture elements in MP halo stars show a behavior that can not be explained using the yields from the main r-process only (Burris et al. 2000). The stars show an increase in the abundance of light s-process (ls) elements (e.g. Sr, Y and Zr) relative to heavy s-process (hs) elements (e.g. Ba) with decreasing metallicity. Our stars show the same behavior. This behavior is not expected if all the n-capture elements in these old stellar populations are produced by the main r-process. Hence it has been proposed in the literature that the ls and hs elements are degenerate at the earliest times before the main s-process in AGB stars kicks in.

Many suggestions exist in the literature for this unknown process, however, so far it is not clear which of these processes is correct. One production site that would contribute to the abundances of ls elements at early times are massive fast-rotating stars (spinstars) (Cescutti et al. 2013). These stars would produce ls elements without producing much of the hs or r-process elements, potentially explaining the behavior seen in MP halo stars.

We compare our results with two GCE models (Cescutti and Chiappini 2014), one for the halo and the other for an old bulge population. These models include the yields from

spinstars as a potential production site for light s-process elements in the early Universe along with the main r-process produced by MRDS. Our comparison to these models show that the models could explain the scatter seen for Sr, Y and Eu, this is not so true for Ba. The interesting result from this comparison, is that the halo model matches our stars much better than the bulge model. This is mostly due to the bulge model having a higher SFR and hence covers higher metallicities, perhaps this is a sign that the current estimates of the bulge's SFR are too high. The results from this comparison show that more work needs to be done to improve the models to better match the observations. The production of the light n-capture elements in the early Universe is yet to be understood.

To conclude this study, our results point toward a similar chemical evolution history for both the halo and the bulge regarding the s-process elements, not so much for the r-process. It is not clear yet whether spinstars were among the first stars or not, hence the source of the early light s-process elements production remains an open question, further work on the theoretical models is needed to see if the yields from spinstars can explain our results. The assumption of the need for a separate production site for the light n-capture elements in the early Universe is based entirely on our currently poor understanding of the r-process, better understanding of the r-process production sites and yields will help in further investigating this topic in the future. The full chemical properties of these stars offer great constraints on the history of the Galaxy and its chemical evolution, once such an analysis is completed, we will be able to get a better understanding of the nature of the first stars and the earliest times in the Galaxy's history.

5.1 Future prospects

This sample of stars gives us a small preview of what lies in the bulge regarding the MP population, increasing the number of MP stars from the bulge with high resolution spectra and high SNR (higher than those of this sample) would be the next step to follow. Key to this would be finding more stars at the lowest metallicities below [Fe/H]$= -3$, we currently have about 20 more stars observed waiting to be analyzed. Measuring the upper limits for stars without Y and Eu would be of great interest, to further investigate the [Y/Sr] behavior as well as to get better statistics on the r-enhancement of our stars.

Howes et al. (2015) showed that some of the stars in our sample are indeed on tight orbits in the inner regions of the Galaxy, however, with the help of Gaia better distances and kinematics for our stars would help in confirming their bulge membership. These old stars provide the best constrains on Galactic chemical evolution models. Accurate and precise abundances using 3D model atmospheres and NLTE radiative transfer analysis would provide better constrains on the nature of the n-capture processes in the early Universe. Given the time, atomic data and model atmospheres, a full 3D NLTE analysis would be highly favored over 1D LTE measurements.

We have only explored the abundances of four n-capture elements, increasing this number will help in getting the full picture regarding the production site/s of n-capture elements in the early Universe. For example, zirconium (Zr) is one of the light s-process elements

that will help in confirming the trends seen for Sr and Y. Another element of interest is lanthanum (La), as it is a heavy s-process element similar to Ba. La abundances would help to ensure the trends seen with Ba are robust. The full chemical properties of these stars (both heavy and light elements) will also help in figuring out how the first stars died and how massive they were. Taking us a step closer to unraveling the mysteries surrounding the earliest epochs in the Galaxy's history.

The assumption for an early s-process production site or a weak r-process is based entirely on our poor understanding of the r-process, further theoretical studies and observations are needed to confirm the yields and production sites of the r-process. On the other hand to confirm the existence of spinstars among the first stellar generations better models are vital.

Appendix A

Stellar parameters

Table A.1: Information for the 48 stars included in this study. This table shows in order, the name of the star (SMSSJ(RA2000)+(Dec2000)), Galactic longitude (l), Galactic latitude (b), SNR at 4500 Å, the effective temperature (T_{eff}), surface gravity ($\log g$), metallicity ([Fe/H]) and microturbulence (ξ) with uncertainties for each parameter.

Star name (SMSS)	l [°]	b [°]	SNR	Teff [K]	Δ_{Teff} [K]	$\log g$ [dex]	$\Delta_{\log g}$ [dex]	[Fe/H] dex	$\Delta_{[Fe/H]}$ dex	ξ [km/s]	Δ_{ξ} [km/s]
J182637.10-342924.2	-0.68	-10.31	42	5070	160	2.5	0.13	-1.97	0.08	1.33	0.2
J182948.50-341053.9	-0.1	-10.77	36	5274	160	2.82	0.13	-2.47	0.11	2.2	0.2
J182600.10-332531.0	0.24	-9.72	27	4680	160	1.36	0.13	-2.53	0.08	2.36	0.2
J182601.20-332358.3	0.26	-9.72	26	5246	160	1.65	0.12	-2.83	0.11	2.5	0.2
J182753.80-334607.7	0.1	-10.23	19	4842	160	1.53	0.12	-2.31	0.06	2.5	0.2
J183000.40-333919.3	0.4	-10.58	40	4776	160	1.55	0.12	-2.63	0.07	2.45	0.2
J182922.50-335559.4	0.09	-10.58	50	5420	160	1.94	0.12	-2.77	0.08	2.5	0.2
J182930.05-335958.3	0.04	-10.63	17	4952	160	1.25	0.13	-1.97	0.12	2.27	0.2
J183225.30-334938.4	0.46	-11.1	19	5293	160	2.35	0.12	-1.74	0.09	1.79	0.2
J183128.70-341018.4*	0.06	-11.07	22	4940	160	2.15	0.13	-1.83	0.1	1.99	0.2
J182153.85-341018.8*	359.2	-9.3	113	4896	160	1.33	0.12	-2.51	0.07	1.86	0.2
J183617.33-270005.3*	7.1	-8.9	34	4842	160	1.93	0.12	-2.8	0.1	2.05	0.2
J175510.50-412812.1*	350.2	-8	12	5266	160	1.75	0.13	-2.36	0.31	2.26	0.2
J175652.43-413612.8	350.2	-8.4	10	5142	160	3.15	0.13	-2.39	0.13	1.13	0.2
J173823.38-145701.1	11.1	8.7	72	4599	160	0.99	0.15	-3.36	0.1	2.3	0.2
J182048.26-273329.2	5	-6.1	53	4949	160	2.22	0.15	-3.48	0.09	1.9	0.2
J183744.90-280831.1	6.2	-9.7	57	4597	160	0.98	0.13	-2.92	0.07	2.05	0.2
J183647.89-274333.1	6.5	-9.3	43	4649	160	1.17	0.12	-2.48	0.06	2.5	0.2
J183812.72-270746.3	7.1	-9.3	28	4873	160	1.74	0.14	-3.22	0.08	1.81	0.2
J183719.09-262725.0	7.7	-8.9	34	4791	160	1.64	0.13	-3.18	0.07	1.81	0.2
J184201.19-302159.6	4.5	-11.5	59	5136	160	2.55	0.13	-2.84	0.07	1.96	0.2
J184656.07-292351.5	5.9	-12	64	4857	160	1.93	0.13	-2.76	0.07	1.83	0.2
J181406.68-313106.1	0.8	-6.6	47	4821	160	1.48	0.13	-2.82	0.06	1.96	0.2
J181317.69-343801.9	357.9	-7.9	51	5015	160	2.25	0.12	-2.28	0.06	1.48	0.2

Table A.1 Continued:

Star name (SMSS)	l [°]	b [°]	SNR	Teff [K]	Δ_{Teff} [K]	$\log g$ [cgs]	$\Delta_{\log g}$ [cgs]	[Fe/H] dex	$\Delta_{[Fe/H]}$ dex	ξ [km/s]	Δ_{ξ} [km/s]
J181219.68-343726.4	357.9	-7.7	46	4873	160	1.94	0.13	-2.5	0.07	1.93	0.2
J181609.62-333218.7	359.2	-7.9	63	4809	160	1.93	0.19	-3.94	0.16	1.6	0.2
J181634.60-340342.5	358.8	-8.3	60	4821	160	1.61	0.12	-2.46	0.06	1.79	0.2
J175544.54-392700.9	352	-7.1	48	4857	160	1.83	0.12	-2.65	0.07	1.6	0.2
J175455.52-380339.3	353.1	-6.3	72	4714	160	1.1	0.18	-3.36	0.14	1.8	0.2
J175746.58-384750.0	352.8	-7.2	31	5064	160	1.96	0.14	-2.81	0.1	2.36	0.2
J181736.59-391303.3	354.2	-10.8	58	4612	160	1.05	0.13	-2.59	0.09	2.09	0.2
J181505.16-385514.9	354.2	-10.2	45	4962	160	2.73	0.15	-3.29	0.1	2.1	0.2
J181921.64-381429.0	355.2	-10.6	68	4917	160	2.02	0.13	-2.72	0.07	1.94	0.2
J175722.68-411731.8	350.5	-8.3	88	4894	160	1.97	0.13	-2.88	0.07	2.02	0.2
J175021.86-414627.1	349.4	-7.4	93	5015	160	2.12	0.13	-2.6	0.07	1.55	0.2
J175636.59-403545.9	351.1	-7.9	52	4934	160	1.79	0.17	-3.21	0.13	1.96	0.2
J175433.19-411048.9	350.4	-7.8	97	4912	160	1.91	0.15	-3.26	0.11	1.94	0.2
J181815.99-242253.2	7.56	-4.09	32	4768	160	1.43	0.13	-2.72	0.07	1.93	0.2
J170817.27-293928.9	354.86	6.36	27	4664	160	1.21	0.13	-2.3	0.07	2.22	0.2
J165605.96-342646.4	349.46	5.51	34	4632	160	1.06	0.13	-2.48	0.09	1.93	0.2
J181722.18-335209.4	359.02	-8.31	38	4718	160	1.32	0.13	-2.52	0.08	1.87	0.2
J181946.17-340737.3	359.02	-8.88	87	4899	160	2.04	0.13	-2.25	0.06	1.79	0.2
J182051.46-340733.3	359.12	-9.08	65	4792	160	1.64	0.13	-2.38	0.07	1.89	0.2
J175140.30-382955.6	352.42	-5.98	70	4828	160	1.71	0.13	-2.34	0.06	1.76	0.2
J175633.89-414628.6	350.02	-8.42	28	5052	160	2.04	0.13	-2.46	0.11	1.56	0.2
J175610.36-414650.8	349.98	-8.36	42	5178	160	2.93	0.13	-2.34	0.09	1.52	0.2
J175400.31-402621.7	350.96	-7.34	14	5061	160	2.8	0.13	-2.25	0.13	1.42	0.2
J175432.75-410749.6	350.4	-7.77	44	5068	160	1.94	0.13	-2.4	0.08	1.64	0.2

* These stars are observed by UVES on the VLT, the SNR for these stars is measured at 4900Å.

Appendix B

Line list

Table B.1: Atomic data for spectral lines used for abundance determination. Column 1 gives the element and excitation state, the wavelength in Å listed in column 2, column 3 shows the lower level excitation energy and column 4 lists the $\log gf$ values.

Ion	λ (Å)	χ_l (eV)	$\log gf$	Ion	λ (Å)	χ_l (eV)	$\log gf$
Sr II	4077.7090	0.0	0.167	Ba II	6141.7129	0.7036	-0.220
Sr II	4215.5190	0.0	-0.145	Ba II	6141.7129	0.7036	-1.026
Y II	3747.5523	0.1042	-0.910	Ba II	6141.7140	0.7036	-1.181
Y II	3774.3298	0.1296	0.210	Ba II	6141.7143	0.7036	-1.257
Y II	3788.6935	0.1042	-0.070	Ba II	6141.7154	0.7036	-1.693
Y II	3950.3494	0.1042	-0.490	Ba II	6141.7169	0.7036	-3.072
Y II	4398.0103	0.1296	-1.000	Ba II	6141.7183	0.7036	-3.051
Y II	4883.6821	1.0326	0.070	Ba II	6496.8976	0.6043	-1.327
Y II	4900.1189	1.0326	-0.09	Ba II	6496.8977	0.6043	-0.521
Y II	5087.4190	1.0840	-0.17	Ba II	6496.8988	0.6043	-1.482
Y II	5200.4097	0.9923	-0.57	Ba II	6496.8992	0.6043	-1.558
Ba II	4934.0744	0.0	-3.125	Ba II	6496.9004	0.6043	-1.994
Ba II	4934.0744	0.0	-1.331	Ba II	6496.9021	0.6043	-3.373
Ba II	4934.0750	0.0	-3.146	Ba II	6496.9037	0.6043	-3.352
Ba II	4934.0751	0.0	-1.100	Eu II	3819.6610	0.0	0.190
Ba II	4934.0755	0.0	-1.767	Eu II	3819.6830	0.0	0.228
Ba II	4934.0758	0.0	-1.255	Eu II	3907.0950	0.207	-0.150
Ba II	4934.0773	0.0	-0.294	Eu II	3907.1170	0.207	-0.112
Ba II	5853.6741	0.6043	-1.95	Eu II	4129.6940	0.0	-0.100
Ba II	5853.6742	0.6043	-1.144	Eu II	4129.7200	0.0	-0.062
Ba II	5853.6751	0.6043	-2.105	Eu II	4205.0280	0.0	-0.110
Ba II	5853.6753	0.6043	-2.181	Eu II	4205.0540	0.0	-0.072
Ba II	5853.6764	0.6043	-2.617				

Bibliography

Amarsi, A. M., Lind, K., Asplund, M., Barklem, P. S., and Collet, R. (2016). Non-LTE line formation of Fe in late-type stars - III. 3D non-LTE analysis of metal-poor stars. MNRAS, 463:1518–1533.

Andrievsky, S. M., Spite, F., Korotin, S. A., François, P., Spite, M., Bonifacio, P., Cayrel, R., and Hill, V. (2011). NLTE strontium abundance in a sample of extremely metal poor stars and the Sr/Ba ratio in the early Galaxy. A&A, 530:A105.

Argast, D., Samland, M., Thielemann, F.-K., and Qian, Y.-Z. (2004). Neutron star mergers versus core-collapse supernovae as dominant r-process sites in the early Galaxy. A&A, 416:997–1011.

Arlandini, C., Käppeler, F., Wisshak, K., Gallino, R., Lugaro, M., Busso, M., and Straniero, O. (1999). Neutron Capture in Low-Mass Asymptotic Giant Branch Stars: Cross Sections and Abundance Signatures. ApJ, 525:886–900.

Asplund, M. (2005). New Light on Stellar Abundance Analyses: Departures from LTE and Homogeneity. ARA&A, 43:481–530.

Bagnulo, S., Jehin, E., Ledoux, C., Cabanac, R., Melo, C., Gilmozzi, R., and ESO Paranal Science Operations Team (2003). The UVES Paranal Observatory Project: A Library of High- Resolution Spectra of Stars across the Hertzsprung-Russell Diagram. *The Messenger*, 114:10–14.

Barbuy, B., Zoccali, M., Ortolani, S., Hill, V., Minniti, D., Bica, E., Renzini, A., and Gómez, A. (2009). VLT-FLAMES analysis of 8 giants in the bulge metal-poor globular cluster NGC 6522: oldest cluster in the Galaxy?. Analysis of 8 giants in NGC 6522. A&A, 507:405–415.

Barklem, P. S., Christlieb, N., Beers, T. C., Hill, V., Bessell, M. S., Holmberg, J., Marsteller, B., Rossi, S., Zickgraf, F.-J., and Reimers, D. (2005). The Hamburg/ESO R-process enhanced star survey (HERES). II. Spectroscopic analysis of the survey sample. A&A, 439:129–151.

Beers, T. C. and Christlieb, N. (2005). The Discovery and Analysis of Very Metal-Poor Stars in the Galaxy. ARA&A, 43:531–580.

Bland-Hawthorn, J. and Gerhard, O. (2016). The Galaxy in Context: Structural, Kinematic, and Integrated Properties. ARA&A, 54:529–596.

Bromm, V. and Larson, R. B. (2004). The First Stars. ARA&A, 42:79–118.

Burris, D. L., Pilachowski, C. A., Armandroff, T. E., Sneden, C., Cowan, J. J., and Roe, H. (2000). Neutron-Capture Elements in the Early Galaxy: Insights from a Large Sample of Metal-poor Giants. ApJ, 544:302–319.

Busso, M., Gallino, R., and Wasserburg, G. J. (1999). Nucleosynthesis in Asymptotic Giant Branch Stars: Relevance for Galactic Enrichment and Solar System Formation. ARA&A, 37:239–309.

Caffau, E., Bonifacio, P., François, P., Spite, M., Spite, F., Zaggia, S., Ludwig, H.-G., Monaco, L., Sbordone, L., Cayrel, R., Hammer, F., Randich, S., Hill, V., and Molaro, P. (2011). X-Shooter GTO: chemical analysis of a sample of EMP candidates. A&A, 534:A4.

Casey, A. R. (2014). *A Tale of Tidal Tales in the Milky Way*. PhD thesis, Australian National University.

Cescutti, G. and Chiappini, C. (2014). Explaining the Ba, Y, Sr, and Eu abundance scatter in metal-poor halo stars: constraints to the r-process. A&A, 565:A51.

Cescutti, G., Chiappini, C., Hirschi, R., Meynet, G., and Frischknecht, U. (2013). The s-process in the Galactic halo: the fifth signature of spinstars in the early Universe? A&A, 553:A51.

Chiappini, C., Frischknecht, U., Meynet, G., Hirschi, R., Barbuy, B., Pignatari, M., Decressin, T., and Maeder, A. (2011). Imprints of fast-rotating massive stars in the Galactic Bulge. Nature, 474:666.

Christlieb, N., Bessell, M. S., Beers, T. C., Gustafsson, B., Korn, A., Barklem, P. S., Karlsson, T., Mizuno-Wiedner, M., and Rossi, S. (2002). A stellar relic from the early Milky Way. Nature, 419:904–906.

Cowan, J. J. and Thielemann, F.-K. (2004). R-Process Nucleosynthesis in Supernovae. *Physics Today*, 57(10):47–53.

Diemand, J., Madau, P., and Moore, B. (2005). The distribution and kinematics of early high-σ peaks in present-day haloes: implications for rare objects and old stellar populations. MNRAS, 364:367–383.

François, P., Depagne, E., Hill, V., Spite, M., Spite, F., Plez, B., Beers, T. C., Andersen, J., James, G., Barbuy, B., Cayrel, R., Bonifacio, P., Molaro, P., Nordström, B., and Primas, F. (2007). First stars. VIII. Enrichment of the neutron-capture elements in the early Galaxy. A&A, 476:935–950.

Frebel, A., Aoki, W., Christlieb, N., Ando, H., Asplund, M., Barklem, P. S., Beers, T. C., Eriksson, K., Fechner, C., Fujimoto, M. Y., Honda, S., Kajino, T., Minezaki, T., Nomoto, K., Norris, J. E., Ryan, S. G., Takada-Hidai, M., Tsangarides, S., and Yoshii, Y. (2005). Nucleosynthetic signatures of the first stars. Nature, 434:871–873.

Frebel, A. and Norris, J. E. (2015). Near-Field Cosmology with Extremely Metal-Poor Stars. ARA&A, 53:631–688.

Frebel, A., Simon, J. D., Kirby, E., Geha, M., and Willman, B. (2010). Extremely metal-poor stars in dwarf galaxies. In Cunha, K., Spite, M., and Barbuy, B., editors, *Chemical Abundances in the Universe: Connecting First Stars to Planets*, volume 265 of *IAU Symposium*, pages 237–240.

Freeman, K. and Bland-Hawthorn, J. (2002). The New Galaxy: Signatures of Its Formation. ARA&A, 40:487–537.

Freiburghaus, C., Rosswog, S., and Thielemann, F.-K. (1999). R-Process in Neutron Star Mergers. ApJ, 525:L121–L124.

Gray, D. F. (2008). *The Observation and Analysis of Stellar Photospheres*. Cambridge University Press.

Grevesse, N., Asplund, M., and Sauval, A. J. (2007). The Solar Chemical Composition. Space Sci. Rev., 130:105–114.

Gustafsson, B., Edvardsson, B., Eriksson, K., Jørgensen, U. G., Nordlund, Å., and Plez, B. (2008). A grid of MARCS model atmospheres for late-type stars. I. Methods and general properties. A&A, 486:951–970.

Heiter, U., Jofré, P., Gustafsson, B., Korn, A. J., Soubiran, C., and Thévenin, F. (2015a). Gaia FGK benchmark stars: Effective temperatures and surface gravities. A&A, 582:A49.

Heiter, U., Lind, K., Asplund, M., Barklem, P. S., Bergemann, M., Magrini, L., Masseron, T., Mikolaitis, Š., Pickering, J. C., and Ruffoni, M. P. (2015b). Atomic and molecular data for optical stellar spectroscopy. Phys. Scr, 90(5):054010.

Howes, L. M., Asplund, M., Casey, A. R., Keller, S. C., Yong, D., Gilmore, G., Lind, K., Worley, C., Bessell, M. S., Casagrande, L., Marino, A. F., Nataf, D. M., Owen, C. I., Da Costa, G. S., Schmidt, B. P., Tisserand, P., Randich, S., Feltzing, S., Vallenari, A., Allende Prieto, C., Bensby, T., Flaccomio, E., Korn, A. J., Pancino, E., Recio-Blanco, A., Smiljanic, R., Bergemann, M., Costado, M. T., Damiani, F., Heiter, U., Hill, V., Hourihane, A., Jofré, P., Lardo, C., de Laverny, P., Magrini, L., Maiorca, E., Masseron, T., Morbidelli, L., Sacco, G. G., Minniti, D., and Zoccali, M. (2014). The Gaia-ESO Survey: the most metal-poor stars in the Galactic bulge. MNRAS, 445:4241–4246.

Howes, L. M., Asplund, M., Keller, S. C., Casey, A. R., Yong, D., Lind, K., Frebel, A., Hays, A., Alves-Brito, A., Bessell, M. S., Casagrande, L., Marino, A. F., Nataf, D. M., Owen, C. I., Da Costa, G. S., Schmidt, B. P., and Tisserand, P. (2016). The EMBLA survey - metal-poor stars in the Galactic bulge. MNRAS, 460:884–901.

Howes, L. M., Casey, A. R., Asplund, M., Keller, S. C., Yong, D., Nataf, D. M., Poleski, R., Lind, K., Kobayashi, C., Owen, C. I., Ness, M., Bessell, M. S., da Costa, G. S., Schmidt, B. P., Tisserand, P., Udalski, A., Szymański, M. K., Soszyński, I., Pietrzyński, G., Ulaczyk, K., Wyrzykowski, Ł., Pietrukowicz, P., Skowron, J., Kozłowski, S., and Mróz, P. (2015). Extremely metal-poor stars from the cosmic dawn in the bulge of the Milky Way. Nature, 527:484–487.

Ishimaru, Y., Wanajo, S., and Prantzos, N. (2015). Neutron Star Mergers as the Origin of r-process Elements in the Galactic Halo Based on the Sub-halo Clustering Scenario. ApJ, 804:L35.

Ji, A. P., Frebel, A., Chiti, A., and Simon, J. D. (2016). R-process enrichment from a single event in an ancient dwarf galaxy. Nature, 531:610–613.

Jofré, P., Heiter, U., Soubiran, C., Blanco-Cuaresma, S., Worley, C. C., Pancino, E., Cantat-Gaudin, T., Magrini, L., Bergemann, M., González Hernández, J. I., Hill, V., Lardo, C., de Laverny, P., Lind, K., Masseron, T., Montes, D., Mucciarelli, A., Nordlander, T., Recio Blanco, A., Sobeck, J., Sordo, R., Sousa, S. G., Tabernero, H., Vallenari, A., and Van Eck, S. (2014). Gaia FGK benchmark stars: Metallicity. A&A, 564:A133.

Käppeler, F., Gallino, R., Bisterzo, S., and Aoki, W. (2011). The s process: Nuclear physics, stellar models, and observations. *Reviews of Modern Physics*, 83:157–194.

Karlsson, T., Bromm, V., and Bland-Hawthorn, J. (2013). Pregalactic metal enrichment: The chemical signatures of the first stars. *Reviews of Modern Physics*, 85:809–848.

Keller, S. C., Bessell, M. S., Frebel, A., Casey, A. R., Asplund, M., Jacobson, H. R., Lind, K., Norris, J. E., Yong, D., Heger, A., Magic, Z., da Costa, G. S., Schmidt, B. P., and Tisserand, P. (2014). A single low-energy, iron-poor supernova as the source of metals in the star SMSS J031300.36-670839.3. Nature, 506:463–466.

Keller, S. C., Schmidt, B. P., Bessell, M. S., Conroy, P. G., Francis, P., Granlund, A., Kowald, E., Oates, A. P., Martin-Jones, T., Preston, T., Tisserand, P., Vaccarella, A., and Waterson, M. F. (2007). The SkyMapper Telescope and The Southern Sky Survey. PASA, 24:1–12.

Maeder, A. and Meynet, G. (2012). Rotating massive stars: From first stars to gamma ray bursts. *Reviews of Modern Physics*, 84:25–63.

Ness, M., Freeman, K., Athanassoula, E., Wylie-de-Boer, E., Bland-Hawthorn, J., Asplund, M., Lewis, G. F., Yong, D., Lane, R. R., and Kiss, L. L. (2013). ARGOS - III. Stellar populations in the Galactic bulge of the Milky Way. MNRAS, 430:836–857.

Pignatari, M., Gallino, R., Meynet, G., Hirschi, R., Herwig, F., and Wiescher, M. (2008). The s-Process in Massive Stars at Low Metallicity: The Effect of Primary ^{14}N from Fast Rotating Stars. ApJ, 687:L95.

Piskunov, N. and Valenti, J. A. (2017). Spectroscopy Made Easy: Evolution. A&A, 597:A16.

Roederer, I. U., Preston, G. W., Thompson, I. B., Shectman, S. A., Sneden, C., Burley, G. S., and Kelson, D. D. (2014). A Search for Stars of Very Low Metal Abundance. VI. Detailed Abundances of 313 Metal-poor Stars. AJ, 147:136.

Salvadori, S., Ferrara, A., Schneider, R., Scannapieco, E., and Kawata, D. (2010). Mining the Galactic halo for very metal-poor stars. MNRAS, 401:L5–L9.

Sneden, C., Cowan, J. J., and Gallino, R. (2008). Neutron-Capture Elements in the Early Galaxy. ARA&A, 46:241–288.

Stacy, A. and Bromm, V. (2014). The First Stars: A Low-mass Formation Mode. ApJ, 785:73.

Starkenburg, E., Oman, K. A., Navarro, J. F., Crain, R. A., Fattahi, A., Frenk, C. S., Sawala, T., and Schaye, J. (2017). The oldest and most metal-poor stars in the APOSTLE Local Group simulations. MNRAS, 465:2212–2224.

Stoehr, F., White, R., Smith, M., Kamp, I., Thompson, R., Durand, D., Freudling, W., Fraquelli, D., Haase, J., Hook, R., Kimball, T., Kümmel, M., Levay, K., Lombardi, M., Micol, A., and Rogers, T. (2008). DER_SNR: A Simple & General Spectroscopic Signal-to-Noise Measurement Algorithm. In Argyle, R. W., Bunclark, P. S., and Lewis, J. R., editors, *Astronomical Data Analysis Software and Systems XVII*, volume 394 of *Astronomical Society of the Pacific Conference Series*, page 505.

Travaglio, C., Gallino, R., Arnone, E., Cowan, J., Jordan, F., and Sneden, C. (2004). Galactic Evolution of Sr, Y, And Zr: A Multiplicity of Nucleosynthetic Processes. ApJ, 601:864–884.

Tumlinson, J. (2010). Chemical Evolution in Hierarchical Models of Cosmic Structure. II. The Formation of the Milky Way Stellar Halo and the Distribution of the Oldest Stars. ApJ, 708:1398–1418.

Valenti, J. A. and Piskunov, N. (1996). Spectroscopy made easy: A new tool for fitting observations with synthetic spectra. A&AS, 118:595–603.

Wehmeyer, B., Pignatari, M., and Thielemann, F.-K. (2015). Galactic evolution of rapid neutron capture process abundances: the inhomogeneous approach. MNRAS, 452:1970–1981.

White, S. D. M. and Springel, V. (2000). Where Are the First Stars Now? In Weiss, A., Abel, T. G., and Hill, V., editors, *The First Stars*, page 327.

Yong, D., Norris, J. E., Bessell, M. S., Christlieb, N., Asplund, M., Beers, T. C., Barklem, P. S., Frebel, A., and Ryan, S. G. (2013). The Most Metal-poor Stars. II. Chemical Abundances of 190 Metal-poor Stars Including 10 New Stars with [Fe/H] = -3.5. ApJ, 762:26.